Graz University of Technology

Integral invariants for robust geometry processing.

Helmut Pottmann, Johannes Wallner, Qi-Xing Huang, and Yong-Liang Yang

Integral Invariants for Robust Geometry Processing

Helmut Pottmann
TU Wien

Johannes Wallner
TU Graz

Qi-Xing Huang
Stanford University

Yong-Liang Yang
Tsinghua University

Abstract

Differential invariants of curves and surfaces such as curvatures and their derivatives play a central role in Geometry Processing. They are, however, sensitive to noise and minor perturbations and do not exhibit the desired multi-scale behaviour. Recently, the relationships between differential invariants and certain integrals over small neighborhoods have been used to define efficiently computable integral invariants which have both a geometric meaning and useful stability properties. This paper considers integral invariants defined via distance functions, and the stability analysis of integral invariants in general. Such invariants proved useful for many tasks where the computation of shape characteristics is important. A prominent and recent example is the automatic reassembling of broken objects based on correspondences between fracture surfaces.

Keywords: geometry processing, curvature, integral invariant, stability, 3D shape understanding

1 Introduction

Local shape analysis of curves and surfaces usually employs concepts of elementary differential geometry like curvatures (see e.g. [do Carmo 1976; Porteous 2001]). Likewise, global shape understanding benefits from differential geometry concepts like principal curvature lines or crest lines (see for instance [Alliez et al. 2003; Hildebrandt et al. 2005; Kim and Kim 2005; Ohtake et al. 2004; Yokoya and Levine 1989]). However, the actual computation of curvatures for real data, given as triangle meshes or voxel grids, is a nontrivial task, because numerical differentiation is sensitive to noise. A standard method to deal with rough data is denoising and smoothing prior to numeric computation. These techniques come in two categories: Global methods which employ appropriate geometric flows (cf. [Bajaj and Xu 2003; Clarenz et al. 2004b; Osher and Fedkiw 2002]) and local ones, which use approximation by smooth surfaces (cf. [Taubin 1995; Cazals and Pouget 2003; Goldfeather and Interrante 2004; Ohtake et al. 2004; Razdan and Bae 2005]). We especially want to mention the method of tensor voting (cf. [Tong and Tang 2005]). Semi-differential invariants in the sense of [Van Gool et al. 1992] are a way of avoiding higher derivatives by combining reference points with first order derivatives.

An alternative approach to differential geometry for meshes is to employ an exact theory of discrete analogues of differential quantities, instead of numerically approximating the smooth theory. This area of research, which could be called discrete differential geometry in a narrower sense, has been investigated for a long time, and many results have been achieved – see e.g. work by [Aleksandrov and Zalgaller 1967], [Cheeger et al. 1984], [Pinkall and Polthier 1993], [Bobenko and Pinkall 1996], [Polthier 2002], [Meyer et al. 2002], [Cohen-Steiner and Morvan 2003], [Bobenko and Schröder 2005]. It is possible to deal with noisy data using such discrete theories, as shown by [Hildebrandt and Polthier 2004], [Rugis and Klette 2006], and [Rusinkiewicz 2004]. However, handling noisy data appears to be neither the main strength nor the original intent of an entirely discrete theory.

Typically a discrete theory of curvatures associates them to vertices or edges or faces in a mesh, and such a discrete curvature often

has an interpretation, e.g. as 'curvature concentrated in a vertex', or 'integral of curvature over a face'. This measure-theoretic interpretation of curvatures should not be confused with the integral invariants of the present paper.

Our approach to the numerical problems inherent in the computation of higher order differential invariants of noisy geometry is the following: For given 3D data, we integrate various functions over suitable small kernel domains like balls and spheres, which yields *integral invariants* associated with each kernel location. These invariants turn out to have a geometric meaning and can be used as curvature estimators. This method has been initiated by [Manay et al. 2004] and [Connolly 1986] and is also the topic of [Yang et al. 2006; Pottmann et al. 2007].

The following properties of curvature estimators are important:

- Robustness with respect to noise, including discretization artifacts;

- Multi-scale behaviour, i.e., adaptability to the choice of resolution.

Integration, which is an essential ingredient in the definition of integral invariants, has a smoothing effect and achieves stability and robustness without the need for preprocessing.

The present paper studies robustness aspects of integral invariants, as well as integral invariants related to distance functions. Thus we establish the theoretical explanation of robustness properties encountered in numerical experiments and geometry processing algorithms. For the volume descriptor and similar invariants the relation to shape (i.e., curvatures) have already been established; we here present this analysis for geometry descriptors based on distance functions.

1A Prior Work

The first to introduce integral invariants were [Manay et al. 2004]. One example is the *area invariant* suitable for estimating the curvature of a curve c at a point $\mathbf{p}$, where c is assumed to be the boundary of a planar domain D (see Fig. 1, left): Consider the circular disk $B_r(\mathbf{p})$ of radius r and center $\mathbf{p}$, and compute the area $A_r(\mathbf{p})$ of the intersection $B_r(\mathbf{p}) \cap D$. The relation between $A_r(\mathbf{p})$ and the curva-
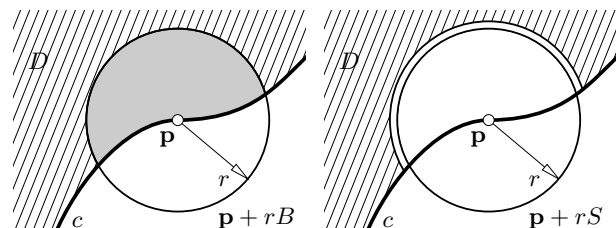

Figure 1: Examples of simple integral invariants for planar curves which are defined by means of disks $\mathbf{p} + rB$ and circles $\mathbf{p} + rS$ centered in a point $\mathbf{p}$. The area invariant (left) is the surface area of the intersection of the disk $\mathbf{p} + rB$ with the domain D, whereas the Connolly function (right) is the perimeter of the arc $(\mathbf{p} + rS) \cap D$ divided by r.

ture yields a way to estimate curvature *at scale r*, because features smaller than r hardly influence the result of computation. Manay et al. show the superior performance of this and other integral invariants on noisy data, especially for the reliable retrieval of shapes from geometric databases.

A similar invariant appears in earlier work (see Fig. 1, right): The angle of the circular arc $\partial B_r(\mathbf{p}) \cap D$ has been used by [Connolly 1986] for molecular shape analysis. If we multiply this so-called Connolly function by the kernel radius r, we obtain the length of the circular arc, which happens to be the derivative of the area invariant with respect to the kernel radius.

The extensions of area invariant and Connolly function to surfaces in three-space are straightforward. One arrives at the volume descriptor, whose relation to mean curvature is derived by [Hulin and Troyanov 2003], and which is used by [Gelfand et al. 2005] for global surface matching. Its derivative with respect to r is the surface area of the spherical patch $\partial B_r(\mathbf{p}) \cap D$ (see [Connolly 1986]). The precise relation between these integral invariants on the one hand, and the curvature of planar curves and the mean curvature on surfaces on the other hand, has been derived by [Cazals et al. 2003].

Principal component analysis of the domain $B_r(\mathbf{p}) \cap D$ is done by integrating coordinate functions and their products over that domain. Therefore also principal moments of inertia and principal directions of $B_r(\mathbf{p}) \cap D$ are integral invariants. A discussion of their relation to principal curvatures and of computational issues is given by [Pottmann et al. 2007], while [Yang et al. 2006] shows applications and compares this method with other ways of estimating principal curvatures. We also point to [Clarenz et al. 2004b; Clarenz et al. 2004a], who use principal component analysis of surface patches for feature detection.

Results of a similar flavour, without the emphasis on computability and robustness, are the formulae of J. Bertrand and V. A. Puiseux (1848) which relate Gaussian curvature to perimeter and area of geodesic disks (cf. p. 127 of [Strubecker 1969]).

1B Organization and main contributions of the present paper

Our paper is organized as follows: After introducing notation and some basic facts in sections 2 and 3, we briefly discuss integral invariants for planar curves in Section 4. Those are mainly the *area invariant* and its derivatives with respect to kernel radius and kernel center, respectively. The analogous but slightly more involved discussion of the 3D counterparts, namely the volume descriptor and its derivatives, is performed in Section 5. Section 6 studies invariants for curves in surfaces and shows how to obtain the geodesic curvature by integration. Invariants based on distance functions are the topic of Section 7 – both for surfaces and for space curves. Section 8 analyzes the stability of some important integral invariants in the presence of noise or surface perturbations. Section 9 is concerned with efficient computation and implementation issues. Applications are briefly surveyed in Section 10. We conclude our paper with Section 11, which contains pointers to future research.

The main contributions of the present paper are (i) new facts about asymptotics expansion of integral invariants and their relations to curvature, notably those computed from distance functions (ii) a thorough theoretical stability and robustness analysis of integral invariants, with a focus on the volume descriptor; (iii) methods for computing integral invariants, especially the octree-based approach of Section 9B.

2 Basics

2A Notation and definition of integral invariants

In this paper we assume that a curve in $\mathbb{R}^2$ or a surface in $\mathbb{R}^3$ is the boundary ∂D of a domain D in $\mathbb{R}^n$, with $n = 2, 3$, respectively (locally, this is always the case, so this is no actual restriction). We write 1_D for the indicator function of that domain: $1_D(\mathbf{x}) = 1$ if the point $\mathbf{x}$ is contained in D, and $1_D(\mathbf{x}) = 0$ otherwise.

B denotes the unit ball, and $\mathbf{p} + rB$ denotes the ball with radius r and center $\mathbf{p}$. In $\mathbb{R}^2$, such a ball is actually a disk, but we use the same notation regardless of dimension. Further, the unit circle of $\mathbb{R}^2$ and the unit sphere of $\mathbb{R}^3$ are denoted by S. S is the boundary of B. The symbol $\mathbf{p} + rS$ denotes the sphere or circle with center $\mathbf{p}$ and radius r.

In many cases, integral invariants, evaluated at the boundary point $\mathbf{p}$ of a domain D, have the form of one of the two following convolution integrals:

$$I_r(\mathbf{p}) = \int_{\mathbf{p}+rB} g(\mathbf{x})w(\mathbf{p} - \mathbf{x})d\mathbf{x}, \quad I_r'(\mathbf{p}) = \int_{\mathbf{p}+rS} g(\mathbf{x})w(\mathbf{p} - \mathbf{x})d\mathbf{x}, \quad (1)$$

where g is a function associated with the domain (e.g., its indicator function or the distance from the boundary), and w is a weight function (e.g., a constant). The symbol $d\mathbf{x}$ has various meanings, depending on the domain of integration. E.g. in dimension $n = 3$, when integrating over the domain $\mathbf{p} + rB$, it means a volume integral. In dimension $n = 2$, when integrating over $\mathbf{p} + rS$, it means an arc length integral. In the remaining cases ($n = 3$, integral over a sphere, and $n = 2$, integral over a disk) $d\mathbf{x}$ means an area integral.

As an example, both the area invariant and the Connolly function (cf. Fig. 1) have the general form of Equation (1): we let $g(\mathbf{x}) = 1_D(\mathbf{x})$ and $w(\mathbf{x}) = 1$.

2B Integral invariants as functions of the kernel radius

For geometry processing applications, the multi-scale behaviour of an integral invariant defined by (1) is important, which means the change of its value, if the kernel radius r varies. This leads us to consider integral invariants as univariate functions of the kernel radius. A useful piece of information on these functions is the general relation

$$\frac{d}{dr}I_r(\mathbf{p}) = I_r'(\mathbf{p}), \quad (2)$$

which follows immediately from the product formula for integrals: $I_r(\mathbf{p}) = \int_0^r I_\rho'(\mathbf{p})d\rho$ (see [Pottmann et al. 2007]). Another important topic is the asymptotic behaviour when the kernel radius r tends to zero. [Pottmann et al. 2007] give a general recipe for computing the first few terms in the Taylor expansion of $I_r(\mathbf{p})$. Invariants which are of this type are the area and volume functionals (see below), geometry descriptors based on the distance function (introduced in the present paper), and quantities used in principal component analysis (cf. [Yang et al. 2006; Pottmann et al. 2007]).

2C Integral invariants as functions of the kernel center

When the radius used in the definition of an integral invariant $I_r(\mathbf{p})$ or $I_r'(\mathbf{p})$ is kept constant, then this invariant is a function of the point $\mathbf{p}$. Usually we are interested in the values of the invariant when the point $\mathbf{p}$ is situated on the surface under investigation. The relations between integral invariants and geometric characteristics of the surface (mostly curvatures), which one is interested in, are no longer valid if $\mathbf{p}$ is not contained in the surface.

Nevertheless we are interested in the behaviour of the invariant when $\mathbf{p}$ leaves the surface. The main reason for this is that in actual computations we are often concerned with imprecise or quantized data, and the point for which integral invariants are evaluated may actually lie at some distance from the hypothetical smooth surface under consideration. In order to estimate the effect of these perturbations, we compute the gradient vector $\nabla I_r = (\frac{\partial}{\partial p_1}, \frac{\partial}{\partial p_2}, \frac{\partial}{\partial p_3}) \cdot \int_{\mathbf{p}+rB} g(\mathbf{x})d\mathbf{x}$, and the same for $I'_r(\mathbf{p})$. The magnitude of perturbation is then measured by $I_r(\mathbf{p} + \Delta\mathbf{p}) = I_r(\mathbf{p}) + \langle \Delta\mathbf{p}, \nabla I_r(\mathbf{p}) \rangle + O(2)$, where $O(2)$ denotes second order terms and $\langle\,,\rangle$ is the scalar product of vectors. Consequently, we can give a simple estimate for the change ΔI_r in the integral invariant in terms of the change in the point $\mathbf{p}$: Approximately, $\|\Delta I_r\| \lessapprox \|\Delta\mathbf{p}\| \cdot \|\nabla I_r\|$.

3 Facts about curves and surfaces

This material is found e.g. in the monographs by [do Carmo 1976] or [Spivak 1975]. References for the facts on distance functions quoted below are [Ambrosio and Mantegazza 1998] and [Pottmann and Hofer 2003].

3A Planar curves

For every point $\mathbf{p}$ of a sufficiently smooth curve c we can choose a Cartesian coordinate system with $\mathbf{p}$ as origin, such that the x_1 axis is tangent to the curve (the Frenet frame). With respect to such coordinates, the curve may be written as the graph of a function $x_2 = f(x_1)$, with $f(x_1) = \alpha x_1^2 + \beta x_1^3 + \gamma x_1^4 + O(x_1^5)$. With the well known formula $\kappa = f''(1 + (f')^2)^{-3/2}$ for the curvature we can relate the coefficients in the Taylor expansion with the derivatives of the curvatures; the result is

$$x_2 = \frac{\kappa}{2}x_1^2 + \frac{\kappa'}{6}x_1^3 + \frac{\kappa'' - 3\kappa^3}{24}x_1^4 + O(x_1^5). \qquad (3)$$

Here the derivatives κ' and κ'' of the curvature are with respect to x_1. For $x_1 = 0$ this is also the derivative with respect to arc length. If the curve is of lesser smoothness, this Taylor expansion terminates not with $O(x_1^5)$, but earlier. Because we need it later, we record in this place the coordinate of the intersection points $\mathbf{c}_r^+$ and $\mathbf{c}_r^-$ of this curve with the circle $x_1^2 + x_2^2 = r^2$ (see Fig. 2): $\mathbf{c}_r^+ = (r, \frac{\kappa}{2}r^2) + (\frac{-\kappa^2}{8}, \frac{\kappa'}{6})r^3 + (\frac{-\kappa\kappa'}{12}, \frac{\kappa''}{24})r^4 + O(r^5)$. The coordinates of $\mathbf{c}_r^-$ are found by substituting $-r$ for r in the previous formula.

3B Surfaces

Next, we discuss coordinate systems for surfaces. For every point $\mathbf{p}$ of a sufficiently smooth surface Φ there is a coordinate system with $\mathbf{p}$ as origin, such that the surface can be written as the graph of a function

$$x_3 = \frac{1}{2}(\kappa_1 x_1^2 + \kappa_2 x_2^2) + R(x_1, x_2), \qquad (4)$$

where κ_1, κ_2 are the principal curvatures of the surface in the point $\mathbf{p}$, and the remainder term $R(x_1, x_2)$ is bounded by $|R(x_1, x_2)| \leq C \cdot (\sqrt{x_1^2 + x_2^2})^3$, i.e., it is of third order. Mean curvature H and Gaussian curvature K are defined by $H = \frac{\kappa_1 + \kappa_2}{2}$, $K = \kappa_1\kappa_2$. If the surface is the boundary of the domain D, we assume that the positive x_3 axis points to the inside of D, so that a convex domain gets nonnegative curvatures. The *distance* of a point $\mathbf{x} \in \mathbb{R}^3$ from the surface can be given a sign, depending on whether $\mathbf{x}$ is inside D or outside: $\mathrm{dist}(\mathbf{x}, \Phi) > 0 \iff \mathbf{x} \notin D$. Recall that the distance, signed or not, fulfills the eikonal equation $\|\nabla\mathrm{dist}(\mathbf{x}, \Phi)\| = 1$. A

Taylor approximation of the signed distance function is given by

$$\mathrm{dist}(\mathbf{x}, \Phi) = \frac{1}{2}(\kappa_1 x_1^2 + \kappa_2 x_2^2) - x_3 + O(3), \qquad (5)$$

where $O(3)$ means a third order remainder term (we use $f(\mathbf{x}) = O(k)$ as an abbreviation of $f(x) = O(\|x\|^k)$ as $\|x\| \to 0$). Note that this Taylor expansion does not contain any quadratic terms which involve x_3 (cf. [Ambrosio and Mantegazza 1998; Pottmann and Hofer 2003]).

3C Space curves

A space curve $\mathbf{c}(u)$ has several orthonormal frames associated with it. For the purposes of this paragraph, we assume that u is an arc length parameter, and a dot indicates differentiation with respect to u. Then the Frenet frame $\{\mathbf{t}, \mathbf{h}, \mathbf{b}\}$ is defined by $\mathbf{t} = \dot{\mathbf{c}}$, $\dot{\mathbf{t}} = \kappa\mathbf{h}$, and $\mathbf{b} = \mathbf{t} \times \mathbf{h}$. Here κ is the curvature. Further, $\dot{\mathbf{b}} = -\tau\mathbf{h}$, where τ is the torsion of the curve. By rotation of the Frenet frame about the unit tangent vector $\mathbf{t}$ we get the class of frames $\{\mathbf{t}, \mathbf{e}_1, \mathbf{e}_2\}$ with $\mathbf{e}_1 = \cos\phi\mathbf{h} + \sin\phi\mathbf{b}$ and $\mathbf{e}_2 = -\sin\phi\mathbf{h} + \cos\phi\mathbf{b}$. If we choose the function ϕ such that $\dot{\phi} = -\tau$, then both $\dot{\mathbf{e}}_1$ and $\dot{\mathbf{e}}_2$ are proportional to $\mathbf{t}$, and $\{\mathbf{t}, \mathbf{e}_1, \mathbf{e}_2\}$ is called a rotation-minimizing frame.

Now consider the ruled surface Ψ_1 parametrized by $\mathbf{g}_1(u, v) = \mathbf{c}(u) + v\mathbf{e}_1(u)$. By differentiation we see that the partial derivatives $\mathbf{g}_{1,u}$, $\mathbf{g}_{1,v}$ and therefore the tangent plane of Ψ_1 in the point $\mathbf{g}_1(u, v)$ is spanned by $\mathbf{t}(u)$ and $\mathbf{e}_1(u)$. As there is no dependence on v, the surface is developable. An analogous result is true for the surface Ψ_2 which is defined via $\mathbf{e}_2$. It follows that the planes orthogonal to c are orthogonal to both Ψ_1 and Ψ_2, and therefore

$$\mathrm{dist}(\mathbf{x}, c)^2 = \mathrm{dist}(\mathbf{x}, \Psi_1)^2 + \mathrm{dist}(\mathbf{x}, \Psi_2)^2. \qquad (6)$$

As the surface Ψ_1 is developable, its principal frame in the point $\mathbf{c}(u) = \mathbf{g}_1(u, 0)$ is $\{\mathbf{t}, \mathbf{e}_1, \mathbf{e}_2\}$, with $\mathbf{e}_2$ as normal vector. By Meusnier's theorem, the principal curvatures have the values $\kappa_1 = \kappa\cos\sphericalangle(\mathbf{h}, \mathbf{e}_2) = \kappa\cos(\phi + \pi/2)$ and $\kappa_2 = 0$. For the surface Ψ_2, the principal frame is $\{-\mathbf{t}, \mathbf{e}_2, \mathbf{e}_1\}$, and the principal curvatures have the values $\kappa_1 = \kappa\cos\sphericalangle(\mathbf{h}, \mathbf{e}_1) = \kappa\cos\phi$ and $\kappa_2 = 0$. This information will be useful when computing distance functions.

3D Curves in surfaces

A curve c contained in a surface Φ has an associated *Darboux frame* $\{\mathbf{t}, \mathbf{e}_2, \mathbf{n}\}$, where $\mathbf{t}$ is the unit tangent vector of c, $\mathbf{n}$ is the surface normal vector, and $\mathbf{e}_2 = \mathbf{n} \times \mathbf{t}$. If the curve is traversed with unit speed, then $\dot{\mathbf{t}} = \kappa_g\mathbf{e}_2 + \kappa_n\mathbf{n}$, $\dot{\mathbf{e}}_2 = -\kappa_g\mathbf{t} + \tau_g\mathbf{n}$, and $\dot{\mathbf{n}} = -\kappa_n\mathbf{t} - \tau_g\mathbf{e}_2$. The coefficient functions κ_g, κ_n, τ_g which occur here are the geodesic curvature, normal curvature, and geodesic torsion of the curve c w.r.t. Φ, respectively. In this place we would like to mention the famous Gauss-Bonnet formula: For a closed curve c with interior $D \subset \Phi$, we have the identity $\oint_c \kappa_g = 2\pi - \int_D K(\mathbf{x})\,d\mathbf{x}$, with K as the Gaussian curvature of the surface Φ.

4 Simple invariants for planar curves

4A Area invariant and Connolly function

Given a planar curve c which occurs as the boundary of the planar domain D, and a point $\mathbf{p} \in c$, [Manay et al. 2004] define the *area invariant* as the invariant I_r according to Equation (1) with $g = 1_D$ and $w(\mathbf{x}) = 1 = \mathrm{const.}$, i.e.,

$$A_r(\mathbf{p}) := \int_{\mathbf{p}+rB} 1_D(\mathbf{x})\,d\mathbf{x}. \qquad (7)$$
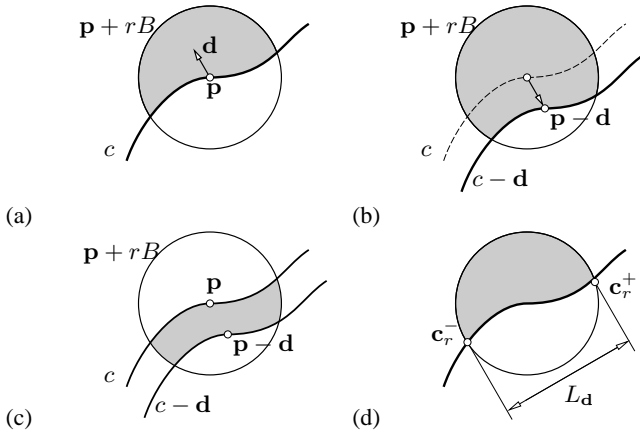
Figure 2: Deriving the gradient of the area invariant. (a) The point $\mathbf{p}$ is moved towards $\mathbf{p} + \mathbf{d}$. (b) This is equivalent to moving the curve c in the opposite direction. (c) The area difference is highlighted. (d) The apparent length $L_{\mathbf{d}}$ of the chord $\mathbf{c}_r^+ - \mathbf{c}_r^-$ when viewed in direction $\mathbf{d}$ contributes to the area difference.

A_r is the area of the intersection $D \cap B_r(\mathbf{p})$ of the curve's interior and the kernel disk $B_r(\mathbf{p})$. The perimeter of the circular arc $D \cap (\mathbf{p} + rS)$ defines the invariant

$$CA_r(\mathbf{p}) := \int_{\mathbf{p}+rS} 1_D(\mathbf{x})\, d\mathbf{x} = \frac{d}{dr} A_r(\mathbf{p}), \qquad (8)$$

(see Fig. 1). The differential relation follows from (2). The name "Connolly function" is given to $CA_r(\mathbf{p})/r$. It has been shown by [Cazals et al. 2003] that there is the Taylor expansion

$$CA_r = \pi r - \kappa r^2 + O(r^3). \qquad (9)$$

By integrating (9), we get

$$A_r = \frac{\pi}{2} r^2 - \frac{\kappa}{3} r^3 + O(r^4). \qquad (10)$$

This is a more precise estimate than $A_r \approx r^3 \arccos(r\kappa/2)$, which was given by [Manay et al. 2004], in the sense that these two expressions have different Taylor expansions as $r \to 0$.

It is worth noting how the behaviour of both the area invariant and the Connolly function changes if the curve under consideration is not smooth. Of course, formulas (9) and (10) are useless. Suppose that the curve c is still smooth, but consists of two curvature continuous pieces joined together at the point $\mathbf{p}$. If left and right limit curvatures have values κ_- and κ_+, then Equation (9) is obviously still valid, with the arithmetic mean of the left and right hand curvature instead of κ. If the curve is not even smooth, but piecewise smooth with an opening angle α different from 180 degrees, then the perimeter of the circular arc which lies inside the curve is shortened or lengthened accordingly, and we arrive at

$$CA_r = \alpha r - \frac{\kappa_- + \kappa_+}{2} r^2 + O(r^3), \qquad (11)$$

$$A_r = \frac{\alpha}{2} r^2 - \frac{\kappa_- + \kappa_+}{6} r^3 + O(r^4), \qquad (12)$$

where the second equation is found by integrating the first one. The case $\alpha = \pi$ and $\kappa_- = \kappa_+ = \kappa$ yields the smooth case.

4B   The gradient of the area functional

Following the general discussion of Section 2C, we are interested in the change of the area invariant $A_r(\mathbf{p})$, if the point $\mathbf{p}$ varies. We pick a direction $\mathbf{d}$ and consider $A_r(\mathbf{p} + \mathbf{d})$. Figures 2.(a)–(d) show the change in area inflicted by the change in $\mathbf{p}$: We have

$$A_r(\mathbf{p} + \mathbf{d}) - A_r(\mathbf{p}) = L_{\mathbf{d}} \cdot \|\mathbf{d}\| + O(\|\mathbf{d}\|^2), \qquad (13)$$

where $L_{\mathbf{d}}$ is the apparent length of the curve segment $c \cap (\mathbf{p} + rB)$ when viewed from direction $\mathbf{d}$ (see Fig. 2).

Denote the two points of intersection of the circle $\mathbf{p} + rS$ with the curve c by $\mathbf{c}_r^-$, $\mathbf{c}_r^+$, and consider the *chord vector*

$$\mathbf{c}_r(\mathbf{p}) = \mathbf{c}_r^+ - \mathbf{c}_r^-. \qquad (14)$$

With the symbol $\mathbf{c}^\perp$ for a rotation about 90 degrees, the apparent length $L_{\mathbf{d}}$ of the curve segment visible in Fig. 2 is now expressed as $L_{\mathbf{d}} = \langle \mathbf{c}_r^\perp, \frac{\mathbf{d}}{\|\mathbf{d}\|} \rangle$. This leads to the following theorem:

Theorem 1 *The gradient of the area invariant $A_r(\mathbf{p})$ with respect to $\mathbf{p}$ is obtained by rotating the chord vector about 90 degrees. The gradient and its norm are expressed by*

$$\nabla_{\mathbf{p}} A_r = \mathbf{c}_r^\perp = (\mathbf{c}_r^+ - \mathbf{c}_r^-)^\perp, \qquad (15)$$

$$\|\nabla A_r(\mathbf{p})\| = 2r - \frac{\kappa^2}{4} r^3 + O(r^4). \qquad (16)$$

Proof. The discussion preceding the theorem implies that the change in area is $\Delta A_r(\mathbf{p}) = \langle \mathbf{c}_r^\perp, \mathbf{d} \rangle + O(2)$, so the area gradient equals $\mathbf{c}_r^\perp$. For the computation of $\|\nabla A_r\| = \|\mathbf{c}_r^+ - \mathbf{c}_r^-\|$ we use the Frenet frame associated with the point $\mathbf{p}$ and the coordinates of $\mathbf{c}_r^+$ and $\mathbf{c}_r^-$ given by Section 3A: We get

$$\mathbf{c}_r = (2r - \kappa^2 r^3/4 + O(r^4), \quad O(r^3))^T \qquad (17)$$

and compute the norm of the gradient: $\|\mathbf{c}_r^\perp\| = \|\mathbf{c}\| = [(2r - \kappa^2 r^3/4 + O(r^4))^2 + O(r^6)]^{1/2} = 2r[1 - \kappa^2 r^2/4 + O(r^4)]^{1/2} = 2r(1 - \kappa^2 r^2/8 + O(r^4))$, by the binomial series. $\square$

The proof of Theorem 1 shows a phenomenon which occurs often when computing with Taylor expansions: The x_1 coordinate of the vector $\mathbf{c}_r$ is known up to third order, whereas the x_2 coordinate has only the general term $O(r^3)$ there. It would appear that we cannot compute the norm up to third order at all. Nevertheless, the computation shows that the third order term in the x_2 coordinate is irrelevant.

5   Simple invariants for surfaces

5A   The volume and surface area descriptors

3D counterparts of the invariants $A_r(\mathbf{p})$, $CA_r(\mathbf{p})$ are the *volume descriptor* $V_r(\mathbf{p})$ and the *surface area descriptor* $SA_r(\mathbf{p})$ of a point $\mathbf{p}$ on the boundary surface of a domain D:

$$V_r(\mathbf{p}) = \int_{\mathbf{p}+rB} 1_D(\mathbf{x})\, d\mathbf{x}, \qquad (18)$$

$$SA_r(\mathbf{p}) = \int_{\mathbf{p}+rS} 1_D(\mathbf{x})\, d\mathbf{x} = \frac{dV_r(\mathbf{p})}{dr}. \qquad (19)$$

The relation of these quantities to mean curvature is discussed in [Hulin and Troyanov 2003] and [Pottmann et al. 2007]:

$$V_r = \frac{2\pi}{3} r^3 - \frac{\pi H}{4} r^4 + O(r^5), \quad SA_r = 2\pi r^2 - \pi H r^3 + O(r^4). \qquad (20)$$
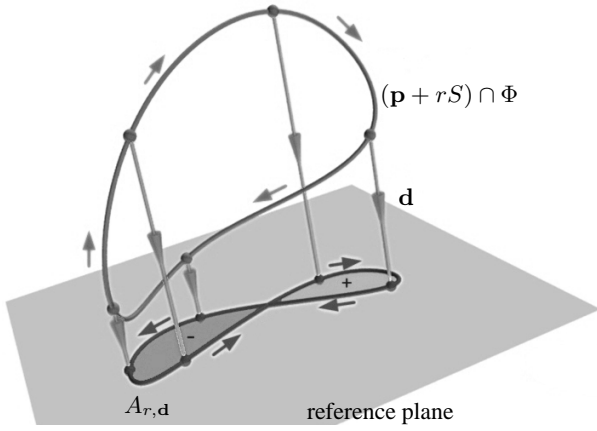
Figure 3: The apparent area $A_{r,\mathbf{d}}$ enclosed by a space curve $(\mathbf{p} + rS) \cap \Phi$ when seen in direction of the vector $\mathbf{d}$ is found as area enclosed by the planar curve which arises when projecting the given space curve onto a reference plane orthogonal to $\mathbf{d}$. The area is endowed with a sign, depending on the orientation of the boundary curve. With the area vector $\mathbf{a}_r$, we have $A_{r,\mathbf{d}} = \langle \mathbf{a}_r, \mathbf{d}/\|\mathbf{d}\| \rangle$.

The normalized sphere area descriptor SA_r/r^2 has been introduced by Connolly [Connolly 1986] for molecular shape analysis. For an application in the same field it has been studied by [Cazals et al. 2003].

Equation (20) can be used to estimate the mean curvature. We define the mean curvature estimators $\widetilde{H}_r(\mathbf{p})$ and $\widetilde{\widetilde{H}}_r(\mathbf{p})$ at scale r by deleting higher order terms in the Taylor expansions in (20):

$$\widetilde{H}_r(\mathbf{p}) = \frac{8}{3r} - \frac{4V_r(\mathbf{p})}{\pi r^4}, \qquad \widetilde{\widetilde{H}}_r(\mathbf{p}) = \frac{2}{r} - \frac{SA_r(\mathbf{p})}{\pi r^3}. \qquad (21)$$

In the limit $r \to 0$, both $\widetilde{H}_r(\mathbf{p})$ and $\widetilde{\widetilde{H}}_r(\mathbf{p})$ tend to the actual mean curvature $H(\mathbf{p})$.

Like in the curve case, we would like to study the behaviour of the volume descriptor for surfaces which are only piecewise smooth and piecewise curvature-continuous. Consider a point $\mathbf{p}$ at a sharp edge, where two smooth surface patches meet. The opening angle of that edge shall be α. In the smooth case (no edge), $\alpha = \pi$. Clearly, the Taylor series of the volume descriptor starts with $2\alpha r^3/3$, but the higher order terms are not so obvious. A more detailed analysis shows that the curvature of the edge relative to the adjoining surfaces is irrelevant for the r^4 term, and that the volume descriptor has the form $V_r = \frac{2\alpha}{3}r^3 - \frac{\pi(H_- + H_+)}{8}r^4 + O(r^5)$. Here H^+ and H^- are the mean curvatures to either side of the edge. The case of a sharp corner is more complicated.

5B The gradient of the volume functional

We are now interested in the gradient $\nabla V_r(\mathbf{p})$ of the volume descriptor with respect to $\mathbf{p}$. We consider the surface Φ which is the boundary of the domain D. As in Section 4B, we choose a direction $\mathbf{d}$ and investigate the difference $V_r(\mathbf{p} + \mathbf{d}) - V_r(\mathbf{p})$. The 2D counterpart of this analysis is illustrated by Fig. 2: the difference of volumes is given by

$$V_r(\mathbf{p} + \mathbf{d}) - V_r(\mathbf{p}) = A_{r,\mathbf{d}}\|\mathbf{d}\| + O(\|\mathbf{d}\|^2), \qquad (22)$$

where $A_{r,\mathbf{d}}$ is the apparent oriented area of the surface patch $\Phi \cap B_r(\mathbf{p})$ when viewed from the direction $\mathbf{d}$. This area is the same as the oriented area enclosed by the projection of the closed curve

$c_r = \Phi \cap \partial B_r(\mathbf{p})$ onto any plane which is orthogonal to $\mathbf{d}$. Let $\mathbf{c}_r(u)$ be a parameterization of this curve c_r on the sphere $S_r^2(\mathbf{p})$. We consider its *area vector*

$$\mathbf{a}_r(\mathbf{p}) = \frac{1}{2} \oint_{c_r} \mathbf{x} \times d\mathbf{x} = \frac{1}{2} \int_I \mathbf{c}_r(u) \times \dot{\mathbf{c}}_r(u)\, du. \qquad (23)$$

It is well known that the apparent area $A_{r,\mathbf{d}}$ can be expressed as $A_{r,\mathbf{d}} = \langle \mathbf{a}_r(\mathbf{p}), \frac{\mathbf{d}}{\|\mathbf{d}\|} \rangle$, which leads to $\Delta V_r(\mathbf{p}) = \langle \mathbf{a}_r(\mathbf{p}), \Delta\mathbf{p} \rangle + O(2)$.

Theorem 2 *The gradient of the volume descriptor $V_r(\mathbf{p})$ with respect to the point $\mathbf{p}$ is the area vector $\mathbf{a}_r(\mathbf{p})$, whose definition in terms of the intersection curve $\Phi \cap (\mathbf{p} + rS)$ is given by Equation (23):*

$$\nabla V_r(\mathbf{p}) = \mathbf{a}_r(\mathbf{p}). \qquad (24)$$

If $\mathbf{n}(\mathbf{p})$ is a unit normal vector of the surface Φ in the point $\mathbf{p}$, which points towards the inside of the domain D, then the area vector has the following Taylor expansion:

$$\mathbf{a}_r(\mathbf{p}) = \pi\left[r^2 - \frac{3H^2 - K}{8}r^4\right]\mathbf{n}(\mathbf{p}) + O(r^5). \qquad (25)$$

Proof. Equation (24) follows directly from the discussion preceding the theorem. In order to investigate the behavior of $\mathbf{a}_r$ for $r \to 0$, we express the intersection curve c_r in the principal frame associated with the point $\mathbf{p}$, and we employ cylinder coordinates (ρ, ϕ, x_3), such that $x_1 = \rho\cos\phi$, $x_2 = \rho\sin\phi$. The point of the curve c_r which lies in the plane $\phi = \text{const}$ according to (4) is found by intersecting the curve $x_3 = \frac{1}{2}(\kappa_1(\rho\cos\phi)^2 + \kappa_2(\rho\sin\phi)^2) + O(\rho^3)$ with the circle $\rho^2 + x_3^2 = r$. From the coordinates of $\mathbf{c}^+(r)$ in Section 3A we read off that this point in cylinder coordinates is given by $\rho(\phi) = r - \frac{1}{8}\kappa_n^2(\phi)r^3 + O(r^4)$, $x_3(\phi) = \frac{1}{2}\kappa_n(\phi)r^2 + O(r^3)$, where $\kappa_n(\phi) = \kappa_1\cos^2\phi + \kappa_2\sin^2\phi$. When we return to Cartesian coordinates, we get a point $\mathbf{c}_r(\phi)$ of the intersection curve, and the area vector is computed by integration: $\mathbf{a}_r(\mathbf{p}) = \frac{1}{2}\int_{\phi=0}^{2\pi} [\rho(\phi)\cos\phi, \rho(\phi)\sin\phi, x_3(\phi)]^T \times \frac{d}{d\phi}[\rho(\phi)\cos\phi, \rho(\phi)\sin\phi, x_3(\phi)]^T$. Carrying out this integration yields Equation (25). $\square$

6 Invariants for curves in surfaces

Section 4A dealt with the area invariant for a planar curve c, which arises as the boundary of a domain D. The area invariant $A_r(\mathbf{p})$ means that part of D whose distance from $\mathbf{p}$ does not exceed r.

The same question can be asked if both the domain D and its boundary curve c are contained in a smooth surface Φ. We define

$$A_r(\mathbf{p}, \Phi) := \text{Area}((\mathbf{p} + rB) \cap \Phi). \qquad (26)$$

It is interesting that the Taylor expansion of this area invariant given by the following theorem does not feature surface curvatures in its first two terms.

Theorem 3 *The area invariant of a curve c contained in a smooth surface Φ has the Taylor expansion*

$$A_r(\mathbf{p}, \Phi) = \frac{\pi}{2}r^2 - \frac{\kappa_g}{3}r^3 + O(r^4), \qquad (27)$$

where κ_g is the signed geodesic curvature of the curve c (i.e., the curvature of the projection of c onto the tangent plane in the point $\mathbf{p}$).

Proof. We use a coordinate frame with $\mathbf{p}$ as origin and x_3 axis orthogonal to Φ. Without loss of generality Φ has the parametrization $x_3 = g(x_1, x_2)$. We use the notation $g_{,i} = \frac{\partial g}{\partial x_i}$ and $\rho = \sqrt{x_1^2 + x_2^2}$. As both the x_1 and x_2 axes are tangent to Φ, $g_{,1} = O(\rho)$, $g_{,2} = O(\rho)$. The surface area differential equals $d\mathbf{x} = \sqrt{1 + g_{,1}^2 + g_{,2}^2}\, dx_1\, dx_2 = (1 + O(\rho^2))dx_1\, dx_2$.

A domain D in the surface has a corresponding domain $\widetilde{D}$ in the x_1, x_2 plane, which arises as projection of D. If the diameter of D is of magnitude $O(\rho^2)$, then the area of D, which is computed as $\int_{\widetilde{D}} d\mathbf{x}$, obviously equals $\int_{\widetilde{D}} dx_1\, dx_2 + O(\rho^4)$.

It follows that we can compute the area invariant $A_r(\mathbf{p}, \Phi)$ to an accuracy of $O(\rho^4)$, if we project the curve c under consideration into the x_1, x_2 plane. The result now follows directly from Equation (10). □

We notice that the last paragraph of the preceding proof shows that the area of the surface patch $\Phi \cap (\mathbf{p} + rB)$ equals

$$A_r(\mathbf{p}) = r^2\pi + O(r^4), \qquad (28)$$

(which is e.g. Equ. (21) of [Pottmann et al. 2007]).

Remark 1 *The area invariant for curves in surfaces employs those points of the surface whose distance from the point $\mathbf{p}$, measured in Euclidean space, does not exceed r. We could also ask for the points whose distance, measured inside the surface Φ, does not exceed r. As it turns out, Theorem 3 remains unchanged. The reason for this is that the area of a geodesic disk (i.e., the points at distance $\leq r$ from $\mathbf{p}$) differs from the area of a Euclidean disk only by a term of magnitude $O(r^4)$: According to the formulae of J. Bertrand and V. A. Puiseux (see p. 127 of [Strubecker 1969]), that area has the expansion $GA_r = \pi r^2 - \frac{\pi}{12} K r^4 + O(r^5)$. Here K is the Gaussian curvature of the surface. We should note that the cost of computing geodesic disks usually is too high to merit their use if all we want to compute is curvatures.*

7 Invariants from distance functions

In applications where we have access to a distance function, it makes sense to employ this function or functions derived from it for the definition of integral invariants. We discuss several ways to do this.

7A Invariants composed from the signed distance

Let $\mathrm{dist}(\mathbf{x}, \Phi)$ be the signed distance function associated with a surface Φ: $\mathrm{dist}(\mathbf{x}, \Phi)$ is positive if $\mathbf{x}$ lies outside the domain bounded by Φ, and negative if $\mathbf{x}$ lies inside. The absolute value of the signed distance equals the distance from Φ in the ordinary sense.

We employ the general method of Equation (1) to define the *signed distance integral* D_r. Letting $g(\mathbf{x}) = \mathrm{dist}(\mathbf{x}, \Phi)$ and $w(\mathbf{x}) = 1$ leads to

$$D_r(\mathbf{p}) = \int_{\mathbf{p} + rB} \mathrm{dist}(\mathbf{x}, \Phi)\, d\mathbf{x}. \qquad (29)$$

The relation of these descriptors to shape characteristics is described as follows:

Theorem 4 *The signed distance integral $D_r(\mathbf{p})$ defined by Equation (29) has the Taylor expansion $D_r = \frac{4\pi H}{15} r^5 + O(r^6)$. Here H is the mean curvature of the surface Φ in the point $\mathbf{p}$.*

Proof. We consider the principal coordinate frame associated with the point $\mathbf{p}$ and the quadratic Taylor polynomial of the signed distance function given by Equation (5). Obviously, $D_r = \int_{rB} \left(-x_3 + \frac{1}{2}(\kappa_1 x_1^2 + \kappa_2 x_2^2) + O(\rho^3) \right) d\mathbf{x}$, with $\rho = (x_1^2 + x_2^2 + x_3^2)^{1/2}$. The volume integral of $O(\rho^3)$ over a volume of size $O(r^3)$ is bounded by $O(r^6)$. Computation of the integrals of the functions x_3, x_1^2, x_2^2 finally yields the expression for D_r. □

Note that the descriptor D_r is related to mean curvature, just as the volume descriptor, which moreover is more stable (see the discussion below). Figure 4 illustrates the similarity between these two descriptors. The sphere integral SD_r corresponding to D_r by differentiation has the Taylor expansion $\frac{4\pi H}{3} r^4 + O(r^5)$.
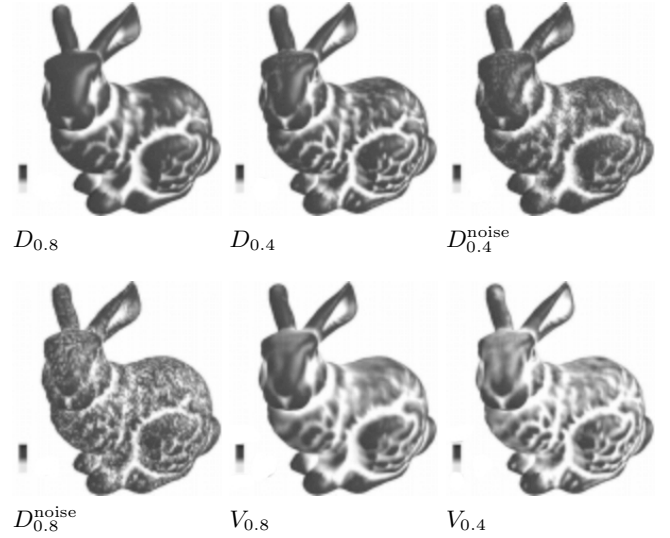

Figure 4: Comparison of the descriptor D_r derived from the signed (un-squared) distance the volume descriptor V_r. Both are related to mean curvature. From top left: D_r for two different kernel radii; D_r for two different kernel radii with artificial noise added; V_r for two different kernel radii. It is clearly visible that all descriptors try to capture the same geometric property (in this case, mean curvature), and that the effect of adding noise is almost eliminated when choosing a bigger neighbourhood for computation. For the kernel ball size compared to the bunny, see Fig. 5.

7B Invariants composed from the squared distance

We now use the *square* of the signed distance function for the definition of integral invariants. We study the *squared distance integral*

$$D_{2,r}(\mathbf{p}) = \int_{\mathbf{p} + rB} \mathrm{dist}(\mathbf{x}, \Phi)^2 d\mathbf{x}, \qquad (30)$$

and the corresponding squared sphere distance integral $SD_{2,r}(\mathbf{p})$ defined by integration over $\mathbf{p} + rS$. The following theorem describes their relation to the curvatures of the surface Φ.

Theorem 5 *The integral invariants $D_{2,r}(\mathbf{p})$ and $SD_{2,r}(\mathbf{p})$ have the Taylor expansions*

$$D_{2,r}(\mathbf{p}) = \frac{4\pi}{15}r^5 - \frac{\pi}{105}(\kappa_1 - \kappa_2)^2 r^7 + O(r^8), \quad (31)$$

$$SD_{2,r}(\mathbf{p}) = \frac{4\pi}{3}r^4 - \frac{\pi}{15}(\kappa_1 - \kappa_2)^2 r^6 + O(r^7). \quad (32)$$

Here κ_1 and κ_2 are the principal curvatures of the surface Φ in the point $\mathbf{p}$.

Proof. It turns out that in order to derive the first two nontrivial terms of the Taylor polynomial of $D_{2,r}(\mathbf{p})$ we need to know the Taylor polynomial of $\operatorname{dist}(\mathbf{x}, \Phi)^2$ up to order four, which can be obtained from a third order Taylor polynomial of $\operatorname{dist}(\mathbf{x}, \Phi)$. We use the principal frame associated with the point $\mathbf{p}$ and write down a third order Taylor polynomial for the surface Φ, thus extending Equation (4):

$$x_3 = \frac{1}{2}(\kappa_1 x_1^2 + \kappa_2 x_2^2) + \frac{1}{6}\sum_{i+j=3} d_{ij0} x_1^i x_2^j + O(4). \quad (33)$$

We are not interested in the geometric meaning of the coefficients d_{ij0}. The 3rd order Taylor polynomial of the signed distance function has the following general form: $\operatorname{dist}(\mathbf{x}, \Phi) = -x_3 + \frac{1}{2}(\kappa_1 x_1^2 + \kappa_2 x_2^2) + \frac{1}{6}\sum_{i+j+k=3} d_{ijk} x_1^i x_2^j x_3^k + O(4)$, where the coefficients d_{ijk} are taken from (33) in case $k = 0$. This is because the zero level set of $\operatorname{dist}(\mathbf{x}, \Phi)$ coincides with the surface described by (33). Once the surface is given, the coefficients d_{ij0} are known, and it turns out that the remaining coefficients d_{ijk} for $k \neq 0$ can be computed by requiring the eikonal equation $\|\nabla \operatorname{dist}(\mathbf{x}, \Phi)\| = 1$ for the distance function. Comparing coefficients $\|\nabla \operatorname{dist}(\mathbf{x}, \Phi)\|^2 = 1$ yields the following expressions for the distance and its square:

$$\operatorname{dist}(\mathbf{x}, \Phi) = -x_3 + \frac{1}{2}(\kappa_1 x_1^2 + \kappa_2 x_2^2) + \frac{x_3}{2}(\kappa_1^2 x_1^2 + \kappa_2^2 x_2^2)$$
$$+ \frac{1}{6}\sum_{i+j=3} d_{ij0} x_1^i x_2^j + O(4),$$

$$\operatorname{dist}(\mathbf{x}, \Phi)^2 = x_3^2 - x_3(\kappa_1 x_1^2 + \kappa_2 x_2^2) - x_3^2(\kappa_1^2 x_1^2 + \kappa_2^2 x_2^2)$$
$$- \frac{x_3}{3}\sum_{i+j=3} d_{ij0} x_1^i x_2^j + \frac{1}{4}(\kappa_1 x_1^2 + \kappa_2 x_2^2)^2 + O(5).$$

Integration over the ball rB yields the formula for $D_{2,r}$, and the one for $SD_{2,r}$ follows by differentiation. Note that the integrals involving the coefficients d_{ij0} are zero. $\qquad\square$

Theorem 5 allows to define estimators $\widetilde{k}^2$ and $\widetilde{\widetilde{k}}^2$ for the squared difference $(\kappa_1 - \kappa_2)^2$ of principal curvatures. We neglect terms of higher order and let

$$\widetilde{k}^2(\mathbf{p}) = \frac{1}{\pi r^7}(28\pi r^5 - 105\, D_{2,r}(\mathbf{p})), \quad (34)$$

$$\widetilde{\widetilde{k}}^2(\mathbf{p}) = \frac{1}{\pi r^6}(20\pi r^4 - 15\, SD_{2,r}(\mathbf{p})). \quad (35)$$

7C   The squared distance from curves in 2D and in 3D

The squared distance function of a planar curve has properties similar to the respective function associated with a surface. Thus it is easy to repeat the discussion of Section 7B for the case of planar curves and derive an analogue of Theorem 5. The extension of this result to space curves is also not difficult, as shown below. Smooth space curves do not separate space into two components, so the distance from a space curve is always considered to be nonnegative.

$D_{2,0.4}$ $D_{2,0.8}$
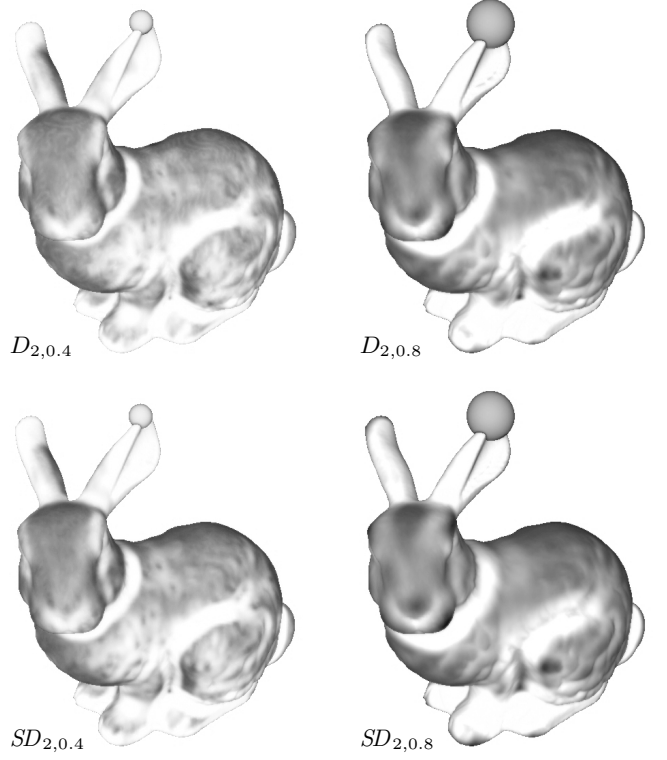
$SD_{2,0.4}$ $SD_{2,0.8}$

Figure 5: Geometry descriptors derived from the squared distance. These figures illustrate the volume integrals $D_{2,r}$ for two different kernel radii, and the surface integrals $SD_{2,r}$, for the same kernel radii. The higher resolution in case of smaller kernel balls is clearly visible. These descriptors estimate the difference of principal curvatures.

Theorem 6 *If c is a planar or spatial curve, the squared distance integral $D_{2,r}(\mathbf{p})$ is related to its curvatures via*

$$\int_{\mathbf{p}+rB} \operatorname{dist}(\mathbf{x}, c)^2 d\mathbf{x} = \frac{\pi}{4}r^4 - \frac{\kappa^2 \pi}{96}r^6 + O(r^7) \text{ or}$$

$$\int_{\mathbf{p}+rB} \operatorname{dist}(\mathbf{x}, c)^2 d\mathbf{x} = \frac{8\pi}{15}r^5 - \frac{\kappa^2 \pi}{105}r^7 + O(r^8),$$

respectively. Here κ is the curvature of c in the point $\mathbf{p}$.

Proof. We use (3) as a starting point to derive a 3rd order Taylor polynomial of the unsigned distance from the curve c. This is completely analogous to the proof of Theorem 5. Its square yields the 4th order approximation of the squared distance:

$$\operatorname{dist}(\mathbf{x}, c)^2 \approx x_2^2 + \kappa^2\left(\frac{x_1^4}{4} - x_1^2 x_2^2\right) - x_2\left(\kappa x_1^2 + \frac{\kappa'}{3}x_1^3\right). \quad (36)$$

This formula is very similar to the corresponding formula for surfaces given above. We integrate this expression over a disk of radius r and get the result for planar curves.

For a space curve c we use (6) to express the squared distance from c as the sum of squared distances from the developable surfaces Ψ_1, Ψ_2 swept by the motion of a rotation-minimizing frame (r.m.f.) $\mathbf{e}_1, \mathbf{e}_2$, as discussed in Section 3C. In the point under consideration, we let the r.m.f. coincide with the Frenet frame, so that $\mathbf{t}, \mathbf{e}_1, \mathbf{e}_2$ and

$\mathbf{t}, \mathbf{e}_2, \mathbf{e}_1$ are principal frames for Ψ_1, Ψ_2, respectively, and these surfaces then have the principal curvatures $(0,0)$ and $(\kappa,0)$ (cf. [do Carmo 1976]).

We now use the proof of Theorem 5 to get Taylor expansion of the distances from Ψ_1 and Ψ_2: $\mathrm{dist}(\mathbf{x}, \Psi_1)^2 = x_3^2 + (\mathrm{odd}) + O(5)$ and $\mathrm{dist}(\mathbf{x}, \Psi_2)^2 = x_2^2 - \kappa^2 x_2^2 x_1^2 + \frac{\kappa^2 x_1^4}{4} + (\mathrm{odd}) + O(5)$. Here "odd" means a linear combination of terms $x_1^i x_2^j x_3^k$ where at least one of i, j, k is odd. Now (6) implies that

$$\mathrm{dist}(\mathbf{x}, c)^2 = x_2^2 + x_3^2 + \kappa^2 \left(\frac{x_1^4}{4} - x_1^2 x_2^2 \right) + (\mathrm{odd}) + O(5). \quad (37)$$

This expression is similar to (36), the only relevant difference being the x_3^2 term. Integration over the ball rB yields the desired result. $\square$

8 Stability analysis

All invariants considered in this paper are obtained by integration rather than by differentiation, which lets us expect robust behaviour with respect to perturbations and noise – at least, a behaviour which is more robust than that of quantities computed by numerical differentiation. In this section we investigate this stability problem from a theoretical perspective. Experimentally, robustness properties have been confirmed by the successful usage of curvature measures derived from integral invariants in algorithms for solving the kinematic registration problem (see e.g. [Gelfand et al. 2005]), for establishing surface correspondences for 3D puzzles (see [Huang et al. 2006]), and others.

Let us start with some general remarks. Our integral invariants (descriptors) compute a value which is defined by a kernel ball and a given surface. Mostly only that part of the surface which lies inside the kernel ball enters the definition. We discuss how the descriptor value changes if either the kernel or the surface undergoes a perturbation. Clearly instead of moving the kernel ball, one could also move the surface in the opposite direction, so we confine ourselves to perturbations of the surface. Without loss of generality we consider only *normal variations* of the form

$$\mathbf{p}^* = \mathbf{p} + \delta(\mathbf{p})\mathbf{n}(\mathbf{p}), \quad (38)$$

where $\mathbf{p}$ is a point on the surface, $\mathbf{n}(\mathbf{p})$ is the unit normal vector of the point $\mathbf{p}$ and pointing outside (with respect to the domain D), and $\delta(\mathbf{p})$ is the amount of perturbation.
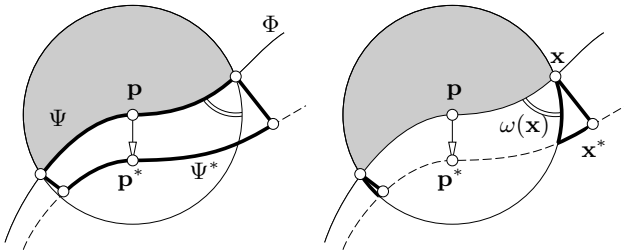

Figure 6: Perturbation $\mathbf{p}^* = \mathbf{p} + \delta(\mathbf{p})\mathbf{n}(\mathbf{p})$ of a surface Φ and its influence on the volume descriptor. Left: The volume ΔV between surface patches Ψ and Ψ^*. Right: Correction volumes V_{corr}.

8A Stability of the volume descriptor: Theory

Stability computations for the volume descriptor are very much related to the volume formula for a normal variation of a surface according to (38): If Ψ is a part of the surface Φ, then the volume

change 'directly over Ψ' (see Fig. 6) has the form

$$\Delta V = \int_{\Psi} \left(\delta - \delta^2 H + \frac{1}{3}\delta^3 K \right) d\mathbf{x}. \quad (39)$$

Here H, K are the mean and Gaussian curvatures, respectively. Note that ΔV is an oriented volume, as δ can be positive or negative. The formula is valid only as long as the surface offsets are regular.

The surface area $A_r(\mathbf{p})$ inside the kernel ball $\mathbf{p} + rB$, which has been computed in Equation (28), is used in the definition of a *mean perturbation* $\overline{\delta}_r$ and a *maximum perturbation* $\delta_{\max}$:

$$\overline{\delta}_r(\mathbf{p}) = \frac{1}{A_r(\mathbf{p})} \int_{\Phi \cap (\mathbf{p}+rB)} \delta(\mathbf{x})\, d\mathbf{x}, \quad (40)$$

$$\delta_{\max} = \max_{\mathbf{x} \in \Phi \cap (\mathbf{p}+rB)} |\delta(\mathbf{x})|. \quad (41)$$

Theorem 7 *If a perturbation $\delta(\mathbf{x})$ is applied to a surface Φ, then the change in the volume descriptor $V_r(\mathbf{p})$ can be expressed in terms of mean curvature H, mean perturbation $\overline{\delta}_r(\mathbf{p})$, and maximum perturbation $\delta_{\max}$. For a zero mean value perturbation (i.e., $\overline{\delta}_r = 0$), we have*

$$|\Delta V_r| \leq r^2 \pi \delta_{\max}^2 \left(|H| + \frac{|\kappa_1| + |\kappa_2|}{4} + O(\delta_{\max}) + O(r) \right). \quad (42)$$

In general,

$$\Delta V_r = r^2 \pi (\overline{\delta}_r + O(\delta_{\max}^2) + O(\overline{\delta} r^2)). \quad (43)$$

Proof. The change in volume when a surface is perturbed, consists of the integral (39) over the surface patch $\Phi \cap (\mathbf{p}+rB)$, illustrated by Fig. 6, left, together with the volume of the ring-shaped part illustrated by Fig. 6, right (correction volume). Any cross section of this correction volume is triangle-shaped of first order. Its area is given by '(baseline times height)/2', i.e.,

$$A_\Delta(\mathbf{x}) = \delta(\mathbf{x})^2 \cot \omega / 2 + O(\delta^3). \quad (44)$$

Here $\mathbf{x}$ is a point of the intersection curve $c_r = \Phi \cap (\mathbf{p}+rS)$. The correction volume therefore reads

$$V_{\mathrm{corr}} = \oint_{c_r} \frac{1}{2}\delta(\mathbf{x})^2 \cot \omega(\mathbf{x})d\mathbf{x} + O(r^2 \delta^3). \quad (45)$$

We want to relate V_{corr} to the mean curvature of Φ. For that purpose, we note that Equ. (19) of [Pottmann et al. 2007] gives the following parameterization of the curve c_r: $\mathbf{c}_r(\phi) = (\rho \cos \phi, \rho \sin \phi, z)$, with $\rho = r + O(r^3)$ and $z = O(r^2)$. By differentiating (4), we get the surface's normal vector in the point $\mathbf{c}_r(\phi)$: $\mathbf{n}_r(\phi) = [-r\kappa_1 \cos \phi + O(r^2), -r\kappa_2 \sin \phi + O(r^2), 1]^T$. The intersection angle $\omega(\phi)$ between surface and sphere then obeys $\sin \omega(\phi) = -\langle \mathbf{n}_r(\phi), \mathbf{c}_r(\phi) \rangle / \|\mathbf{n}_r(\phi)\| \|\mathbf{c}_r(\phi)\|$. By some simple computations it follows that

$$\cot \omega(\phi) = \frac{r}{2}(\kappa_1 \cos^2 \phi + \kappa_2 \sin^2 \phi) + O(r^2). \quad (46)$$

The arc length differential of the curve $\mathbf{c}_r(\phi)$ reads $ds = (1 + O(r^2))d\phi$. We get

$$V_{\mathrm{corr}} = \int_0^{2\pi} \frac{\delta^2}{2} \left(\frac{r}{2}(\kappa_1 \cos^2 \phi + \kappa_2 \sin^2 \phi) + O(r^2) \right)d\phi + O(\cdot)$$

$$\leq \delta_{\max}^2 \frac{r^2 \pi}{4}(|\kappa_1| + |\kappa_2|) + O(r^3 \delta_{\max}^2) + O(r^2 \delta_{\max}^3).$$

Another term which occurs in the computation of the volume change according to (39) is the integral $\int_\Psi \delta^2 H$. If $\mathbf{x}$ is at distance at most r from the midpoint $\mathbf{p}$, then $H(\mathbf{x}) = H(\mathbf{p}) + O(r)$. Therefore,

$$\int_{\Phi \cap (\mathbf{p}+rB)} \delta^2 H d\mathbf{x} \leq \delta_{\max}^2 r^2 \pi H + O(\delta_{\max}^2 r^3). \quad (47)$$

We have now collected sufficient properties of the various integrals involved to show the statement of the theorem. The total volume change is bounded by $|\int_{\Phi \cap (\mathbf{p}+rB)} (\delta + \delta^2 H + O(\delta^3)| + |V_{\text{corr}}|$. The dominant term equals the surface patch area $r^2 \pi (1 + O(r^2))$ times mean perturbation – the dominant error term being the surface integral of $H\delta^2$. The latter is of order $r^2 \delta_{\max}^2$. In case the mean perturbation is zero, the volume change is dominated by $\int \delta H^2 + V_{\text{corr}}$. Thus the theorem is proved. $\square$

Remark 2 *The results of Theorems 7 and 2 agree, which is seen as follows. The gradient vector of the volume descriptor is given by $\pi r^2 \mathbf{n}(\mathbf{p})$ plus higher order terms, where $\mathbf{n}(\mathbf{p})$ is the normal vector of the surface under consideration. When evaluating the volume descriptor not for a boundary point $\mathbf{p}$, but for a point $\mathbf{p} + \Delta\mathbf{p}$, Theorem 2 shows that the change in the volume descriptor approximately equals $\pi r^2 \langle \mathbf{n}, \Delta\mathbf{p} \rangle$. The same value is also given by Theorem 7, since the change $\mathbf{p} \to \mathbf{p} + \Delta\mathbf{p}$ is equivalent to moving the surface by the amount of $\bar{\delta}_r = \langle \Delta\mathbf{p}, \mathbf{n} \rangle$ in orthogonal direction.*

8B Stability of the volume descriptor: Discussion

In order to assess the significance of Theorem 7 and also Theorem 2 which is a special case, we study the effect of a surface perturbation on the mean curvature estimator $\widetilde{H}$ defined by Equation (21). In case of a zero mean perturbation, we get

$$|\Delta \widetilde{H}_r|_{\bar{\delta}_r=0} = \frac{4|\Delta V_r|}{\pi r^4}$$
$$\leq (\frac{\delta_{\max}}{r})^2 (4|H| + |\kappa_1| + |\kappa_2| + O(r) + O(\delta_{\max})). \quad (48)$$

The *relative change* in the mean curvature estimator consequently is given by

$$\frac{|\Delta \widetilde{H}_r|_{\bar{\delta}_r=0}}{\max(\kappa_1, \kappa_2)} \leq (\frac{\delta_{\max}}{r})^2 (6 + O(r) + O(\delta_{\max})). \quad (49)$$

We see that the stability expressed by Theorem 7 and Equations (48), (49) is quite good, when we consider perturbations smaller than the kernel radius, i.e., $\delta_{\max}/r \ll 1$. Zero mean perturbations occur e.g. in the form of noise, and also as discretization artifacts. The stability encountered here is the best for curvature estimators so far.

In the case of a systematic component in the perturbation (i.e., nonzero mean $\bar{\delta}_r(\mathbf{p})$), the change in the mean curvature estimator has the following form:

$$\Delta \widetilde{H}_r \leq \frac{4}{r} \frac{\bar{\delta}_r + O(\delta_{\max}^2) + O(\bar{\delta}_r r^2)}{r}$$
$$\implies \frac{\Delta \widetilde{H}}{\widetilde{H}} \leq 4 \frac{\widetilde{H}^{-1}}{r} \left(\frac{\bar{\delta}_r + O(\delta_{\max}^2)}{r} + O(r\bar{\delta}_r) \right).$$

This shows that the descriptor $\widetilde{H}$ is stable against perturbations of magnitude $\bar{\delta}_r$, if the following two conditions hold:

– (i) $\bar{\delta}_r$ is small compared to the kernel radius r; and
– (ii) the estimated mean curvature radius $\widetilde{H}^{-1}$ is of the same magnitude or smaller than r.

If $\widetilde{H}$ is employed in feature recognition procedures, then a region of higher mean curvature, i.e., a *feature*, is more likely to persist through perturbations than a non-feature. This behaviour is exactly what is needed from a robust curvature estimator.

Remark 3 *The significance of the stability inequalities presented here lies in the fact that robustness against perturbations is quantified in terms of the magnitude of the perturbation alone, without reference to the perturbation's derivatives.*

Remark 4 *This allows to draw a further conclusion: If a real data set can in theory be seen as a perturbation of a much smoother one, then the previous paragraphs apply. Therefore, the mean curvature estimator $\widetilde{H}$ defined via a certain kernel radius r actually measures, with the bounds given above, the mean curvature of this hypothetic smooth surface.*

8C Stability of the sphere area descriptor: Theory

The sphere area descriptor $SA_r(\mathbf{p})$ is the derivative of the volume descriptor $V_r(\mathbf{p})$ with respect to the kernel radius r and thus cannot be expected to have the same amount of stability. One source of instability is a possibly near-tangential intersection between surface and kernel sphere in case of a kernel radius which is of the same magnitude or smaller than the curvature radii of the surface.

If this intersection angle "ω" is known, the deviation of the intersection curve from its unperturbed state can be quantified. In the limit $r \to 0$, the intersection angle tends to 90 degrees, but in general it is unknown. Nevertheless, we first consider the deviation δ_c of the intersection curve as if ω were known. The reason for that is that a bound on the maximum curve perturbation $\delta_{c,\max}$ leads to a reasonable bound on the perturbations inflicted on the sphere area descriptor. By elementary geometry,

$$\delta_c(\mathbf{x}) = \frac{\delta(\mathbf{x})}{\sin \omega} + O(\delta r^2). \quad (50)$$

As the kernel radius tends to zero, Equation (46) together with $1/\sin \omega = \sqrt{1 + \cot^2 \omega}$ implies that $\delta_c(\mathbf{x}) \approx \delta(\mathbf{x})\left(1 + \frac{r^2}{4}(\kappa_1 \cos^2 \phi + \kappa_2 \sin^2 \phi)^2\right)$, where ϕ is the polar angle associated with the intersection point $\mathbf{x}$. We conclude that

$$\delta_{c,\max} \leq \delta_{\max}(1 + O(r^2)) \quad (r \to 0). \quad (51)$$

Note that the previous equation applies only in the limit, and that the magnitude of the quadratic terms depends on the curvatures of the surface.

Theorem 8 *A perturbation $\delta(\mathbf{x})$ of the given surface causes the intersection curve c_r to move sideways by an amount $\delta_c(\mathbf{x})$, the mean value of which is denoted by $\bar{\delta}_c$. The sphere area descriptor $SA_r(\mathbf{p})$ changes via*

$$|\Delta SA_r(\mathbf{p})|_{\bar{\delta}_c=0} \leq \pi r \delta_{c,\max}^2 \left(\frac{|H|}{2} + O(r) + O(\delta_{c,\max}) \right) \quad (52)$$
$$\Delta SA_r(\mathbf{p}) = 2\pi r \bar{\delta}_c \left(1 + O(r^2) + O(\delta_{c,\max})\right)$$

depending on whether we have zero mean noise ($\bar{\delta}_c = 0$) or a systematic error ($\bar{\delta}_c \neq 0$). Here H is the mean curvature. As $r \to 0$, replacing the curve perturbation δ_c by the surface perturbation δ in formula (52) causes ΔSA_r to be multiplied by a factor of magnitude $1 + O(r^2)$.

Proof. We consider an arc length parametrization $\mathbf{c}_r(s)$ of the intersection curve c_r, and associate the Darboux frame $\{\mathbf{t}, \mathbf{e}_2, \mathbf{n}\}$ with it (see Section 3D). As we use a coordinate system where the center of the kernel sphere is the origin, the normal vector $\mathbf{n}(\mathbf{x})$ simply equals $-\frac{1}{r}\mathbf{x}$. It follows that $\dot{\mathbf{n}} = \frac{1}{r}\dot{\mathbf{c}}$, i.e., in the notation of Section 3D, $\kappa_n = -1/r$ and $\tau_g = 0$. The perturbation causes $\mathbf{c}(s)$ to move to the point $\widetilde{\mathbf{c}}(s)$, which has the general form

$$\widetilde{\mathbf{c}}(s) = \mathbf{c}(s)\cos\delta_s(s) + r\mathbf{e}_2(s)\sin\delta_s(s),$$

where the amount of perturbation is not expressed in terms of chord length (that would be δ_c) but rather in terms of a polar angle δ_s. Obviously we have $r\delta_s = \delta_c$ of first order, and we also have $\delta_c \leq r\delta_s$. The exact relation follows from expanding the definition $\delta_c(s) := \|\widetilde{\mathbf{c}}(s) - \mathbf{c}(s)\|$ and reads $\delta_c(s) = r\delta_s(s)(1 + O(\delta_c^2))$. The change in surface area now is the oriented area of the spherical domain parametrized by $\mathbf{x}(s, v) = \cos v\, \mathbf{c}(s) + r\sin v\, \mathbf{e}_2(s)$, for $s \in [0, L_r]$ and $v \in [0, \delta_s(s)]$. The surface area element can be written as

$$\begin{aligned} dA &= \det(\mathbf{n}, \mathbf{x}_s, \mathbf{x}_v)\, dv ds \\ &= \det(\mathbf{n}, \mathbf{t}\cos v + r\kappa_g\mathbf{t}\sin v, -\mathbf{c}\sin v + \mathbf{e}_2 r\cos v)\, dv ds \\ &= (r\cos^2 v - r^2\kappa_g\sin v\cos v)\, dv ds \end{aligned}$$

(subscripts indicate differentiation, and we have used the formulae of Section 3D). It follows that the change in surface area $\Delta SA_r(\mathbf{p}) = \int_{s=0}^{L_r}\int_{v=0}^{\delta_s(s)} dA$ equals

$$\begin{aligned} \Delta SA_r(\mathbf{p}) &= \oint_{c_r}\left[r\frac{\sin 2\delta_s + 2\delta_s}{4} - r^2\kappa_g\frac{1 - \cos 2\delta_s}{4}\right] ds \\ &= \oint_{c_r}\left[r\delta_s - r^2\kappa_g\frac{\delta_s^2}{2} + O(r\delta_s^3)\right] ds. \end{aligned}$$

Here we have terminated the sine and cosine series at their quadratic terms. The Gauss-Bonnet theorem $\oint\kappa_g = 2\pi - SA_r/r^2$ and the Taylor expansion $SA_r = 2\pi r^2 - \pi H r^3 + O(r^4)$ together imply that $\oint r^2\kappa_g = \pi H r + O(r^2)$. As to $\oint r\delta_s$ we note that according to Equ. (25) of [Pottmann et al. 2007], the perimeter of the path of integration equals $L_r = 2\pi r + O(r^3)$, and the mean value $\overline{\delta}_c$ is defined to equal $\frac{1}{L_r}\oint\delta_c$. Thus, $\oint r\delta_s = \oint\delta_c(1+O(\delta_c^2)) = 2\pi r(1 + O(r^2))(\overline{\delta}_c + O(\delta_{c,\max}^3)) = 2\pi r\overline{\delta}_c + O(r\delta_{c,\max}^3) + \overline{\delta}_c O(r^3)$. By summing up the cases $\overline{\delta}_c = 0$ and $\overline{\delta}_c \neq 0$ we get Equations (52). By (51) and the discussion preceding that formula, $\delta_{c,\max} = \delta(1+O(r^2))$, so the statement about the limit case $r \to 0$ follows. $\square$

8D   Stability of the sphere area descriptor: Discussion

In order to investigate how good or bad the inequalities (52) are, we now consider robustness from the viewpoint of the curvature estimator $\widetilde{\widetilde{H}}_r$, which is based on the descriptor SA_r. A perturbation of the surface Φ causes a change $\Delta\widetilde{\widetilde{H}}_r = \Delta SA_r/\pi r^3$. Consequently,

$$\frac{|\Delta\widetilde{\widetilde{H}}_r|_{\overline{\delta}=0}}{H} \leq \frac{1}{2}\left(\frac{\delta_{c,\max}}{r}\right)^2 + \cdots, \quad \frac{\Delta\widetilde{\widetilde{H}}_r}{H} = 2\frac{\overline{\delta}_c}{r}\frac{H^{-1}}{r} + \cdots, \tag{53}$$

where higher order terms are not written down. These equations show that the robustness inherent in the sphere area descriptor is nominally the same as for the volume descriptor (see Section 8B). The difference is that we use the perturbation δ_c of the intersection curve instead of the surface perturbation δ. Only asymptotically, $\delta_c \approx \delta$.

8E   Stability of the squared distance integral

So far we have considered stability only for invariants which are related to mean curvature. Fortunately, the squared distance integral $D_{2,r}$ which has a relation not to mean curvature, but to $\kappa_1 - \kappa_2$, also exhibits sufficient stability for practical purposes. If the perturbed surface Φ^* is at distance $\leq \epsilon$ from the original surface Φ, then obviously $|\mathrm{dist}(\mathbf{x}, \Phi^*) - \mathrm{dist}(\mathbf{x}, \Phi)| < \epsilon$. With the implication

$$|d - d^*| \leq \epsilon \implies |d^2 - d^{*2}| = |d - d^*|(d + d^*) \leq \epsilon(2d + \epsilon)$$

the difference of squared distance integrals with respect to Φ and Φ^* reads

$$\Delta D_{2,r}(\mathbf{p}) \leq \epsilon\int_{\mathbf{p}+rB}(2|\mathrm{dist}(\mathbf{x}, \Phi)| + \epsilon)d\mathbf{x} = 2\epsilon D_r^+ + \epsilon^2\frac{4\pi r^3}{3}.$$

Here the quantity D_r^+ is the integral of the *unsigned* distance function over the kernel ball. It would not be hard to relate it to curvatures, using the Taylor expansion of the signed distance function given in this paper, and the general method, presented by [Pottmann et al. 2007], of integrating functions over that part of a kernel ball which lies to one side of the given surface. However, it is obvious that the dominant term in D_r^+ is given by the integral of $|x_3|$ over the kernel ball rB, i.e., $\frac{\pi r^4}{2}$.

We investigate the effect of a surface perturbation in the geometry descriptor $\widetilde{k}$, which is based on $D_{2,r}$, and which estimates $|\kappa_1 - \kappa_2|$. From (34) we get

$$\Delta(\widetilde{k}^2) \approx \Delta D_{2,r}(\mathbf{p})\frac{105}{\pi r^7} \approx \frac{105}{r^2}\left(\frac{\epsilon}{r} + \frac{4}{3}\left(\frac{\epsilon}{r}\right)^2\right). \tag{54}$$

As $\widetilde{k}$ estimates a difference in curvatures, it has to be compared to the curvature of the kernel sphere, i.e., r^{-1}. We therefore rewrite the previous equation as

$$\frac{\Delta(\widetilde{k}^2)}{(0.0975\, r)^{-2}} \approx \frac{\epsilon}{r}\left(1 + \frac{4}{3}\frac{\epsilon}{r}\right). \tag{55}$$

Again, we consider perturbations with $\epsilon \ll r$. We see that the right hand side is bounded in terms of ϵ/r. In contrast to the mean curvature estimators $\widetilde{H}$ and $\widetilde{\widetilde{H}}$, the robustness inequality for $\widetilde{k}$ relates the change in the geometry descriptor to the kernel radius, and not to the value of the geometry descriptor itself.

Another difference to the geometry descriptors derived from volume and sphere area is that here the case of zero mean noise ($\overline{\delta} = 0$) does not lead to better robustness. This is easily explained from the fact the perturbation inflicted on the distance field associated with the surface essentially depends on the mean of $|\delta|$ and not on the mean of δ (see Fig. 7).

Even if we can give bounds for the effect of noise and perturbations, invariants which involve the distance function are generally less stable than those which integrate just the indicator function.

9   Computation of integral invariants

Throughout the paper we maintain the notion that the curves and surfaces under consideration are the boundary of some domain D. This appears to restrict discussion to closed curves and surfaces. All open curves and surfaces however locally occur as part of the boundary of some domain, so this assumption is not a real restriction. Implementing the computation of integral invariants for such 'open' curves and surfaces does not differ in essential ways from
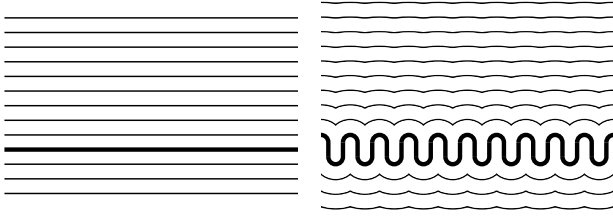
Figure 7: Isolines of the distance function from a curve. Left: unperturbed (straight) line. Right: perturbed version of curve. Apparently the fact that a perturbation has zero mean does not favorably influence the perturbation of the distance field.

doing the same for closed curves and surfaces, and so our discussion will be restricted to the 'closed' case.

The computation of integral invariants for discrete surfaces needs appropriate data structures for preprocessing, as well as intelligent ways of discretizing integrals. We approach this problem in three different ways, each of them being suitable for certain kinds of integral invariants. These are an FFT-based method (Section 9A), an octree based method (Section 9B), and a triangulation based method (Section 9C). We will discuss applications in Section 10.

9A   Computing invariants with FFT

The general form of an integral invariant $I_r(\mathbf{p})$ as defined by (1) can be written in convolution notation. We use the notation 1_{rB} for the indicator function of the ball $r \cdot B$ and write

$$k(\mathbf{x}) = w(\mathbf{x}) \cdot 1_{rB}(\mathbf{x}) \implies$$
$$I_r(\mathbf{p}) = \int_{\mathbb{R}^3} g(\mathbf{x})k(\mathbf{p} - \mathbf{x}) = (g \star k)(\mathbf{p}). \tag{56}$$

Into this category fall the invariants V_r, D_r, $D_{2,r}$, and also the invariants employed in principal component analysis by [Pottmann et al. 2007]. An obvious way to evaluate integral invariants would be to approximate these continuous convolutions by discrete ones and employ FFT for them. This method is also described by [Yang et al. 2006]. Here we are going to show a modification of this simple procedure which yields a better approximation of the continuous convolution.

In our setting, functions are typically only known at grid points $\mathbf{j} \in \mathbb{Z}^3$ with integer coordinates $\mathbf{j} = (j_1, j_2, j_3)$, however we 'know' that they are smooth or have at least smooth level sets. Of course, the continuous convolution $f \star g$ can be approximated by the discrete convolution defined by $(f \circledast g)(\mathbf{k}) = \sum_{\mathbf{j} \in \mathbb{Z}^3} f(\mathbf{j})g(\mathbf{k} - \mathbf{j})$. We will not use this simple approximation, but rather define continuous functions from discrete data and show to evaluate their continuous convolution using the discrete one. Discrete convolutions are computed with FFT.

One way to define a continuous function $g(\mathbf{x})$ from discrete data $g(\mathbf{j})$ is to interpolate between the grid points by letting

$$g(\mathbf{x}) = \sum_{\mathbf{j}} g(\mathbf{j})K(\mathbf{x} - \mathbf{j}), \text{ where} \tag{57}$$
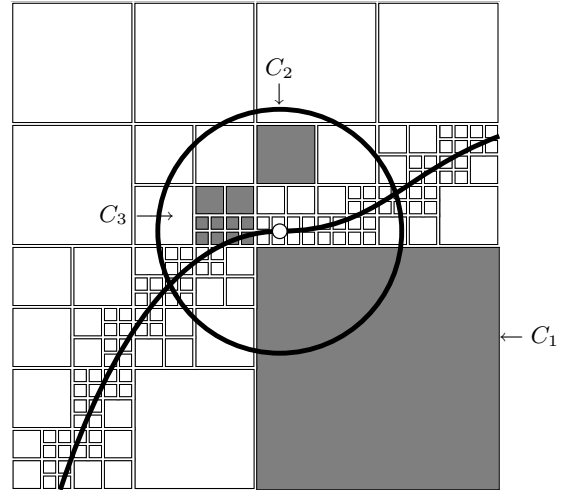$$K(\mathbf{x}) = b(x_1)b(x_2)b(x_3), \ b(\xi) = \max(0, 1 - |\xi|).$$

Figure 8: Integral invariant computation based on an octree data structure. The cubes C_1, C_2, C_3 correspond to cases 2cα, 2b, and 2cβ of Algorithm 1, respectively.

The convolution of (56) now takes the form

$$(g \star k)(\mathbf{p}) = \int \sum_{\mathbf{j}} g(\mathbf{j})K(\mathbf{x} - \mathbf{j})k(\mathbf{p} - \mathbf{x})d\mathbf{x}$$
$$= \sum_{\mathbf{j}} g(\mathbf{j}) \int K(\mathbf{y})k(\mathbf{p} - \mathbf{y} - \mathbf{j})d\mathbf{y}$$
$$= \sum_{\mathbf{j}} g(\mathbf{j})(K \star k)(\mathbf{p} - \mathbf{j}) = (g \circledast (K \star k))(\mathbf{p}).$$

The discrete Fourier transform of $K \star k$, which is needed here, can be precomputed.

The function in the definition of the integral invariant may coincide with the indicator function 1_D of the domain D (in case of the volume descriptor). Knowledge of all values $g(\mathbf{j})$ for integer grid points $\mathbf{j}$ then means that the domain D is voxelized and given as an occupancy grid. We refer to [Gelfand et al. 2005] for more details on the computation of occupancy grids via scan conversion (see e.g. [Nooruddin and Turk 2003]). For the invariant D_r, the function g is the signed distance from the surface under consideration, and for the invariant $D_{2,r}$, we use the square of that distance function. Distance fields can be computed in various ways; we used fast sweeping (see e.g. [Danielsson 1980], [Kimmel et al. 1996], [Tsai et al. 2003], [Zhao 2005], [Kao et al. 2005]).

When we employ FFT for computing discrete convolutions, we actually compute many more values than are necessary, because integral invariants are only evaluated at boundary points of the domain D. In order to reduce computational costs, we invoke convolution not for a single bounding box of D, but for a sequence of boxes which cover the boundary ∂D. We estimate that for box size b the cost of each convolution equals $C(b, r) := N(b, r)^3 \log N(b, r)$ with $N(b, r) = b + 2r$. The total cost then equals $C(b, r)$ times the number of boxes, i.e., is proportional to $C(b, r)/b^2$. Minimizing this function leads to an optimal box size of $b_{\text{opt}}(r) \approx 2.28r$, which for practical purposes gets rounded up such that we apply FFT to a box whose size is a power of two.

9B   An octree based method for computing invariants

An advantage of the FFT method is its simplicity. Disadvantages are that even with an optimized box size we still compute many values which do not interest us, and most importantly, that we can

evaluate integral invariants only at grid points. This section describes a data structure which yields a new way of evaluating integral invariants for the actual surface points.

We decompose an appropriate bounding box of the given surface into a hierarchical collection (an octree) of cubes, such that the function $g(x)$ of Equation (1) is sufficiently well approximated by a quadratic function $\widetilde{g}_i$ in each leaf cube. This approach works well if the function w in Equ. (1) is constant. An example of such a decomposition, with the purpose of computing the volume descriptor, is illustrated by Fig. 8.

Given a decomposition of space into cubes C_i, we write the integral of Equation (1) as follows:

$$M_{i,\mathbf{p}}^r := C_i \cap (\mathbf{p} + rB) \implies$$
$$I_r(\mathbf{p}) = \sum\nolimits_{i: C_i \subseteq (\mathbf{p}+rB)} \Big(\int_{C_i} g\Big) + \sum\nolimits_{\substack{i \,:\, M_{i,\mathbf{p}}^r \neq \emptyset, \\ C_i \nsubseteq (\mathbf{p}+rB)}} \Big(\int_{M_{i,\mathbf{p}}^r} g\Big).$$

It is the aim of our data structure to eliminate integrals of the second kind and adaptively decompose space such that the majority of computations is for integrals of the first type. This is because their values can be precomputed. Integrals of the second kind are computed via the previously obtained approximations $\widetilde{g}_i$ in each leaf cube C_i.

We now describe the three main parts of our method: octree construction, preprocessing, and computation of integral invariants. We focus on the cases $g = 1_D$ (so $I_r(\mathbf{p})$ is the volume descriptor) and the squared distance function.

In the case $g = 1_D$, we construct the octree using a scan conversion method if ∂D is given as a triangle mesh (cf. [Nooruddin and Turk 2003; Ju 2004]), and the method of [Frisken et al. 2000] if it is a point cloud. The function $\widetilde{g}_i$ which approximates the indicator function 1_D in each cube is chosen as a constant, which indicates to which extent the cube C_i lies inside D. As cubes which contain the boundary ∂D are very small anyway, this is a reasonable simplification.

For computing integral invariants based on the squared distance, we have $g(\mathbf{x}) = \text{dist}(\mathbf{x}, \partial D)^2$. In our examples, the values of $g(\mathbf{x})$ have been obtained by fast sweeping (cf. [Tsai et al. 2003; Zhao 2005; Kao et al. 2005]). Then we use the procedure of [Mitra et al. 2004] to determine the decomposition of space into cubes C_i such that within each leaf cube C_i, the squared distance is approximated by quadratic functions $\widetilde{g}_i$.

After the octree has been constructed, we compute the integrals of the function g over each leaf cube C_i, using the approximation $\widetilde{g}_i$, and then propagate these values to obtain the integrals of the function g over the remaining cubes. The computation of $I_r(\mathbf{p})$ runs as sketched in Algorithm 1.

The different types of cubes are illustrated by Figure 8. The most costly operation obviously is to integrate the function $\widetilde{g}_i$ over the domain $C_i \cap (\mathbf{p} + rB)$ in 2cα. This is made easier by the fact that the functions $\widetilde{g}_i$ are actually quadratic. When computing the volume invariant, such that this integral equals the volume of $C_i \cap (\mathbf{p} + rB) \cap D$, the boundary of D can be replaced by its tangent plane if C_i is small.

9C   Computing surface integrals

For the computation of invariants defined by an area integral over the sphere, we employ triangulations of the sphere, and take care of the boundary of the spherical patch we are integrating on. This method is described by [Yang et al. 2006] and [Pottmann et al. 2007], so we do not give details here.

---

1. Initialize C_i with the root cube; let $I = 0$.
2. For the cube C_i, perform the following computations:
    2a. If C_i is outside $\mathbf{p} + rB$, do nothing.
    2b. Else if $C_i \subseteq (\mathbf{p} + rB)$, increase I by the value $\int_{C_i} \widetilde{g}_i$, which is precomputed.
    2c. Else:
        (α) If C_i is a leaf cube, increase I by the value $\int_{C_i \cap (\mathbf{p}+rB)} \widetilde{g}_i$.
        (β) Else, call 2. for all 8 child cubes of C_i.
3. I contains the result.

Algorithm 1.   Computing $I_r(\mathbf{p})$ based on the octree decomposition illustrated by Figure 8.

9D   Computational efficiency

Computation times for the bunny and dragon models from the Stanford collection are indicated in the table below. Here 'preprocessing' for volume integrals means computing a grid structure which stores the characteristic function. For invariants computed by surface integration, a triangulation of the sphere with 13592 triangles has been employed. The run times shown are for a 2 GHz PC with 2 GB RAM. For the volume integrals we have used the method of 9B, for the surface integrals the method of 9C.

model	bunny	dragon
# triangles	69451	104568
grid size for 1_D	$170 \times 168 \times 146$	$194 \times 156 \times 124$
preprocessing	4.6 s	4.4 s
computing V_r	3.8 s	3.7 s
computing SA_r	9.7 s	19.6 s

As to the *squared distance integral*, the preprocessing stage the distance field is computed (we used fast sweeping), takes longer than for the volume descriptor. In the case of the bunny (cf. the table above), this preprocessing step needed 10s.

The cost of computation of integral invariants at n different scales with the FFT method is not proportional to the cost of computing once, but roughly proportional to the cost of $n + 1$ FFTs. E.g. [Huang et al. 2006] computed integral invariants for 8 different radii for the parts of of Fig. 10. This computation needed approximately 1 minute for 400 000 vertices on a 1.4 GHz PC with 512 MB RAM.

10   Applications

We think that integral invariants may be useful for every kind of computation or algorithm which makes use of shape characteristics, especially curvatures. Usually the computation of such geometric properties via integral invariants is rather more robust with respect to perturbations and noise than other methods. For certain integral invariants this experimental result, for which we refer to [Yang et al. 2006], is confirmed by the theoretical investigations of the present paper.

A second property of integral invariants which make them valuable for applications is that they allow to compute at a certain scale r, which for the current paper is identified with the kernel ball radius. The nature of computation is such that surface features smaller than r are considered as noise and will be smoothed out.

There are several publications which deal with applications and comparison of methods, so we will not go into details here (one

Figure 9: Feature extraction on multiple scales according to [Yang et al. 2006]. Integral invariants for several different kernel radii are used to identify features. Darker regions are classified as features on all scales, lighter shaded regions correspond to features extracted at only one or two scales. At left: ravines; at right: ridges. The integral invariants used for this figure are $I_r(x_ix_j)$ $(i,j=1,2,3)$, whose properties are not discussed in the present paper.

of these is [Yang et al. 2006]). Figure 9 illustrates feature detection at multiple scales: ravines and ridges are detected by computing curvatures; and that curvature computation is done by evaluating integral invariants defined by a certain kernel ball of radius r. Features which persist for several values of r are considered to be detected with higher confidence than those which are only detected for a small number of kernel ball radii.

Another application of integral invariants in general is the computation of the network of principal curvature lines in a robust way by [Liu et al. 2006].

A third and important application of integral invariants is the computation of shape characteristics for the purpose of kinematic registration and establishing correspondences between surfaces. Such surfaces can be partially overlapping scan data of the same model – the task is then to merge these scans together in order to create a dataset of the entire object (cf. [Gelfand et al. 2005]). Another instance where the kinematic registration problem occurs in the automatic reassembling of fragments of broken objects by [Huang et al. 2006]. For this '3D puzzle' problem (see Fig. 10), each fragment is represented as a geometric model, e.g., as a triangle mesh, but it is unknown a priori how the pieces fit together. The paper by [Huang et al. 2006] describes a rather involved procedure which recognizes fracture surfaces and finds correspondences between them in order to reestablish the lost connectivity of the original 3D volume. This method relies heavily on the availability of independent and robustly computable geometry descriptors. A significant number of the descriptors involved are integral invariants described in the present paper, namely $V_r(\mathbf{p})$ and $D_{2,r}(\mathbf{p})$, for a sequence of different values of the kernel radius r.

11 Conclusion and future research

We analyzed geometry descriptors, which are capable of capturing shape characteristics, and which exhibit a multi-scale behaviour useful for recognizing persistent features. We discussed theoretical stability results which express again the numerical robustness of integral invariants already encountered in various algorithms. The volume descriptor exhibits the best stability, because compared to invariants based on surface integrals it is averaging over a greater domain, and compared to invariants based on distance functions it is averaging a function whose values which are not subject to noise.
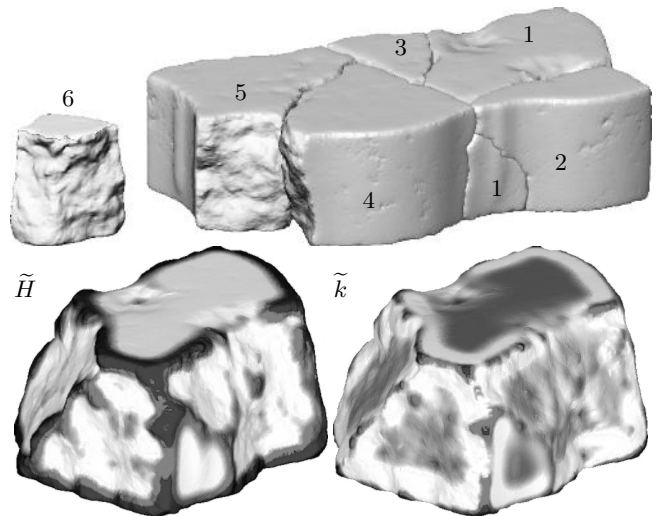

Figure 10: Reassembling a broken brick. The top figure shows all 6 pieces, 5 of them already put together. The figures below shows piece No. 6, with the values of an estimated mean curvature derived from the volume descriptor (at left), and an estimated difference between principal curvatures, derived from the squared distance descriptor. These shape characteristics are employed in order to distinguish fracture surfaces from the smoother surface of the original object, and then to establish correspondences between fracture surfaces for the purpose of automatic reassembling. This figure was taken from [Huang et al. 2006].

Regarding computational efficiency, all invariants described in the present paper generate running times of the same magnitude.

We expect further applications where integral invariants can greatly improve robustness of algorithms. We would like to mention one area of future research which seems promising, namely *shape signatures*. They have been initiated by [Manay et al. 2004]. The signature of a planar curve c is defined as set of points $(I(\mathbf{p}), I'(\mathbf{p}))$, where $\mathbf{p} \in c$, I is a certain integral invariant and I' is its derivative with respect to arc length. In order to enhance robustness, we might want to avoid a derivative, but instead employ another integral invariant I_2. I_2 could be of the same type as I, only computed with respect to a different kernel ball radius. Ideally, the signature should characterize the shape within some tolerance up to rigid body motions (or other transformations). We are not aware of any result in this direction. Clearly, all these investigations should eventually be performed for 3D objects.

Acknowledgements

References

ALEKSANDROV, A. D., AND ZALGALLER, V. A. 1967. *Intrinsic geometry of surfaces*, vol. 15 of *Translations of Mathematical Monographs*. American Mathematical Society.

ALLIEZ, P., COHEN-STEINER, D., DEVILLERS, O., LÉVY, B., AND DESBRUN, M. 2003. Anisotropic polygonal remeshing. *ACM Trans. Graphics 22*, 3, 485–493. Proc. SIGGRAPH.

AMBROSIO, L., AND MANTEGAZZA, C. 1998. Curvature and distance function from a manifold. *J. Geom. Anal. 8*, 723–748.

BAJAJ, C., AND XU, G. 2003. Anisotropic diffusion on surfaces and functions on surfaces. *ACM Trans. Graphics 22*, 1, 4–32.

BOBENKO, A., AND PINKALL, U. 1996. Discrete isothermic surfaces. *J. Reine Angew. Math. 475*, 187–208.

BOBENKO, A., AND SCHRÖDER, P. 2005. Discrete Willmore flow. In *Symp. Geometry Processing*, Eurographics Assoc., M. Desbrun and H. Pottmann, Eds., 101–110.

CAZALS, F., AND POUGET, M. 2003. Estimating differential quantities using polynomial fitting of osculating jets. In *Symp. Geometry Processing*, Eurographics Assoc., L. Kobbelt, P. Schröder, and H. Hoppe, Eds., 177–187.

CAZALS, F., CHAZAL, F., AND LEWINER, T. 2003. Molecular shape analysis based upon the Morse-Smale complex and the Connolly function. In *SCG '03: Proc. 19th Symposium on Computational Geometry*, ACM Press, 351–360.

CHEEGER, J., MÜLLER, W., AND SCHRADER, R. 1984. On the curvature of piecewise flat spaces. *Comm. Math. Phys. 92*, 405–454.

CLARENZ, U., RUMPF, M., SCHWEITZER, M. A., AND TELEA, A. 2004. Feature sensitive multiscale editing on surfaces. *Visual Computer 20*, 5, 329–343.

CLARENZ, U., RUMPF, M., AND TELEA, A. 2004. Robust feature detection and local classification for surfaces based on moment analysis. *IEEE Trans. Vis. Comp. Graphics 10*, 5, 516–524.

COHEN-STEINER, D., AND MORVAN, J. M. 2003. Restricted Delaunay triangulations and normal cycle. In *Proc. 19th annual symposium on Computational geometry*, ACM, 312–321.

CONNOLLY, M. L. 1986. Measurement of protein surface shape by solid angles. *J. Mol. Graph. 4*, 1, 3–6.

DANIELSSON, P.-E. 1980. Euclidean distance mapping. *Computer Graphics and Image Processing 14*, 227–248.

DO CARMO, M. P. 1976. *Differential Geometry of Curves and Surfaces*. Prentice-Hall.

FRISKEN, S. F., PERRY, R. N., ROCKWOOD, A. P., AND JONES, T. R. 2000. Adaptively sampled distance fields: a general representation of shape for computer graphics. In *Proc. SIGGRAPH*, 249–254.

GELFAND, N., MITRA, N. J., GUIBAS, L. J., AND POTTMANN, H. 2005. Robust global registration. In *Symp. Geometry Processing*, Eurographics Assoc., M. Desbrun and H. Pottmann, Eds., 197–206.

GOLDFEATHER, J., AND INTERRANTE, V. 2004. A novel cubic-order algorithm for approximating principal direction vectors. *ACM Trans. Graphics 23*, 1, 45–63.

HILDEBRANDT, K., AND POLTHIER, K. 2004. Anisotropic filtering of non-linear surface features. *Computer Graphics Forum 23*, 3, 391–400. Proc. Eurographics.

HILDEBRANDT, K., POLTHIER, K., AND WARDETZKY, M. 2005. Smooth feature lines on surface meshes. In *Symp. Geometry Processing*, Eurographics Assoc., M. Desbrun and H. Pottmann, Eds., 85–90.

HUANG, Q.-X., FLÖRY, S., GELFAND, N., HOFER, M., AND POTTMANN, H. 2006. Reassembling fractured objects by geometric matching. *ACM Trans. Graphics 25*, 3, 569–578. Proc. SIGGRAPH.

HULIN, D., AND TROYANOV, M. 2003. Mean curvature and asymptotic volume of small balls. *Amer. Math. Monthly 110*, 947–950.

JU, T. 2004. Robust repair of polygonal models. *ACM Trans. Graphics 23*, 3, 888–895. Proc. SIGGRAPH.

KAO, C.-Y., OSHER, S., AND TSAI, Y.-H. 2005. Fast sweeping methods for static Hamilton-Jacobi equations. *SIAM J. Numerical Analysis 42*, 2612–2632.

KIM, S.-K., AND KIM, C.-H. 2005. Finding ridges and valleys in a discrete surface using a modified MLS projection. *Computer-Aided Design 37*, 1533–1542.

KIMMEL, R., KIRYATI, N., AND BRUCKSTEIN, A. M. 1996. Sub-pixel distance maps and weighted distance transforms. *J. Math. Imaging and Vision 6*, 223–233.

LIU, Y., POTTMANN, H., WALLNER, J., YANG, Y.-L., AND WANG, W. 2006. Geometric modeling with conical meshes and developable surfaces. *ACM Trans. Graphics 25*, 3, 681–689. Proc. SIGGRAPH.

MANAY, S., HONG, B.-W., YEZZI, A. J., AND SOATTO, S. 2004. Integral invariant signatures. In *Proc. ECCV 2004/IV*, Springer, T. Pajdla and J. Matas, Eds., vol. 3024 of *Lecture Notes in Computer Science*, 87–99.

MEYER, M., DESBRUN, M., SCHRÖDER, P., AND BARR, A. 2002. Discrete differential-geometry operators for triangulated 2-manifolds. In *Visualization and Math. III*, Springer, H.-C. Hege and K. Polthier, Eds., 35–57.

MITRA, N., GELFAND, N., POTTMANN, H., AND GUIBAS, L. 2004. Registration of point cloud data from a geometric optimization perspective. In *Symp. Geometry Processing*, Eurographics Assoc., R. Scopigno and D. Zorin, Eds., 23–32.

NOORUDDIN, F. S., AND TURK, G. 2003. Simplification and repair of polygonal models using volumetric techniques. *IEEE Trans. Vis. Comp. Graphics 9*, 2, 191–205.

OHTAKE, Y., BELYAEV, A., AND SEIDEL, H.-P. 2004. Ridge-valley lines on meshes via implicit surface fitting. *ACM Trans. Graphics 23*, 3, 609–612. Proc. SIGGRAPH.

OSHER, S., AND FEDKIW, R. 2002. *The Level Set Method and Dynamic Implicit Surfaces*. Springer.

PINKALL, U., AND POLTHIER, K. 1993. Computing discrete minimal surfaces and their conjugates. *Experiment. Math. 2*, 1, 15–36.

POLTHIER, K. 2002. *Polyhedral surfaces of constant mean curvature*. Habilitationsschrift TU Berlin.

PORTEOUS, I. 2001. *Geometric Differentiation*, 2nd ed. Cambridge University Press.

POTTMANN, H., AND HOFER, M. 2003. Geometry of the squared distance function to curves and surfaces. In *Visualization and Mathematics III*, Springer, H.-C. Hege and K. Polthier, Eds., 223–244.

POTTMANN, H., WALLNER, J., YANG, Y.-L., LAI, Y.-K., AND HU, S.-M. 2007. Principal curvatures from the integral invariant viewpoint. *Comput. Aided Geom. Design 24*, 428–442.

RAZDAN, A., AND BAE, M.-S. 2005. Curvature estimation scheme for triangle meshes using biquadratic Bézier patches. *Computer-Aided Design 37*, 1481–1491.

RUGIS, J., AND KLETTE, R. 2006. Surface registration markers from range scan data. In *Combinatorial Image Analysis: 11th int. workshop*, R. Reulke et al., Eds., vol. 4040 of *Lecture Notes Computer Science*. Springer, 430–444.

RUSINKIEWICZ, S. 2004. Estimating curvatures and their derivatives on triangle meshes. In *3D Data Processing, Visualization and Transmission, 2nd Int. Syposium*. IEEE Computer Society, 486–493.

SPIVAK, M. 1975. *A Comprehensive Introduction to Differential Geometry*. Publish or Perish.

STRUBECKER, K. 1969. *Differentialgeometrie: Theorie der Flächenkrümmung*, vol. 1180 of *Sammlung Göschen*. De Gruyter, Berlin.

TAUBIN, G. 1995. Estimating the tensor of curvature of a surface from a polyhedral approximation. In *Proc. Int. Conf. Computer Vision*, 902–907.

TONG, W.-S., AND TANG, C.-K. 2005. Robust estimation of adaptive tensors of curvature by tensor voting. *IEEE Pattern Anal. Machine Intell. 27*, 3, 434–449.

TSAI, Y.-H. R., CHENG, L.-T., OSHER, S., AND ZHAO, H.-K. 2003. Fast sweeping algorithms for a class of Hamilton-Jacobi equations. *SIAM J. Numerical Analysis 41*, 2, 659–672.

VAN GOOL, L. J., MOONS, T., PAUWELS, E., AND OOSTERLINCK, A. 1992. Semi-differential invariants. In *Geometric invariance in computer vision*, J. L. Mundy and A. Zisserman, Eds. MIT Press, 157–192.

YANG, Y.-L., LAI, Y.-K., HU, S.-M., AND POTTMANN, H. 2006. Robust principal curvatures on multiple scales. In *Symp. Geometry processing*, Eurographics Assoc., K. Polthier and A. Sheffer, Eds., 223–226.

YOKOYA, N., AND LEVINE, M. D. 1989. Range image segmentation based on differential geometry: a hybrid approach. *IEEE Trans. Pattern Anal. Machine Intell. 2*, 6, 643–649.

ZHAO, H. 2005. Fast sweeping method for eikonal equations. *Mathematics of Computation 74*, 603–627.